Arms Control and
Treaty Verification
Arms Control and
Treaty Verification
Arms Control and
Treaty Verification
Arms Control and
Treaty Verification
Arms Control and
Treaty Verification
Arms Control and
Treaty Verification
Arms Control and
Treaty Verification
Arms Control and
Treaty Verification
Arms Control and
Treaty Verification
Arms Control and
Treaty Verification
Arms Control and
Treaty Verification
Arms Control and
Treaty Verification
Arms Control and
Treaty Verification
Arms Control and
Treaty Verification
Arms Control and
Treaty Verification
Arms Control and
Treaty Verification
Arms Control and
Treaty Verification
Arms Control and
Treaty Verification
Arms Control and
Treaty Verification

ANL/ACTV-94/1

Plastic-Casting Intrinsic-Surface Unique Identifier (Tag)

by R. G. Palm and A. De Volpi

Argonne National Laboratory, Argonne, Illinois 60439
operated by The University of Chicago
for the United States Department of Energy under Contract W-31-109-Eng-38

Notice
The work reported herein is part of a research and development program for arms control and treaty verification and does not imply current or future policy positions or technical preferences of any agency of the U.S. Government.

Distribution Category:
Nuclear Energy
(UC-940)

ANL/ACTV-94/1

ARGONNE NATIONAL LABORATORY
9700 South Cass Avenue
Argonne, Illinois 60439

Plastic-Casting Intrinsic-Surface Unique Identifier (Tag)

by

R. G. Palm and A. De Volpi*

Reactor Engineering Division

April 1995

Work sponsored by
U.S. Department of Energy
Office of Nonproliferation and National Security

*Technology Development Division

TABLE OF CONTENTS

TABLE OF CONTENTS
(Contd.)

TABLE OF CONTENTS
(Contd.)

LIST OF FIGURES

LIST OF FIGURES
(Contd.)

LIST OF TABLES

ABSTRACT

This report describes the development of an authenticated intrinsic-surface tagging method for unique-identification of controlled items. Although developed for control of items limited by an arms control treaty, this method has other potential applications to keep track of critical or high-value items. Each tag (unique-identifier) consists of the intrinsic, microscopic surface topography of a small designated area on a controlled item. It is implemented by making a baseline plastic casting of the designated tag area and usually placing a cover (for example, a bar-code label) over this area to protect the surface from environmental alteration. The plastic casting is returned to a laboratory and prepared for high-resolution scanning electron microscope imaging. Several images are digitized and stored for use as a standard for authentication of castings taken during future inspections. Authentication is determined by numerically comparing digital images. Commercially available hardware and software are used for this tag. Tag parameters are optimized, so unique casting images are obtained from original surfaces, and images obtained from attempted duplicate surfaces are detected. This optimization uses the modulation transfer function, a first principle of image analysis, to determine the parameters. Surface duplication experiments confirmed the optimization.

I. INTRODUCTION

Beginning in 1988 the Systems and Technology Division of DOE's Office of Arms Control (now the Office of Research and Development of DOE's Office of Nonproliferation and National Security) provided technical support for verification of the proposed START and INF arms-control treaties. Several national laboratories were given the task to develop different unique identifiers (tags). Tamper-indicating tags were believed to have potential as an essential element for accountability of treaty-limited items (TLIs), many of which were mobile.

Tags can have either overt or covert uses. An arms-control treaty would necessarily use an overt tag. A tag is overt when the inspected party has the right to be fully informed about the technology before it will allow its items to be tagged. In addition, for many overt uses the inspected side would have long periods of sole access to the tag. These periods might be used to attempt tag duplication. Tag duplicates could then be placed on uncontrolled items to allow undetected violation of the treaty. Overt tags must be highly resistant to duplication because it may be assumed that the inspected side would have advanced technical capabilities. Covert tags could be considered for uses such as surveillance of export-controlled items. Of course, for the covert mode the adversary would not be aware that an item was tagged, so duplication would not be as important an issue. The most important issue for covert tags is to make them inconspicuous. For many covert applications, the tag reader must also be inconspicuous.

Argonne National Laboratory (ANL) chose to provide unique identification from the surface features of a controlled item. This choice led to use of the scanning electron microscope (SEM) as the authentication instrument. The SEM is preferred, as it is unrivaled in its versatility to examine surfaces. By comparison, an SEM has superior magnification and depth-of-field compared to a light microscope. Several options for SEM surface authentication were initially considered, including attaching an SEM to the item surface.

Given the operational constraints of an arms-control treaty environment, ANL determined that the best option was to capture the tag micro-topography with surface castings and to examine these castings in the SEM. This option is the called the plastic-casting intrinsic-surface tag. The surface casting is made from acetone-soluble cellulose acetate. This is a standard replication technique used to capture sub-micron surface topography. Use of a surface casting for unique-identification of controlled items is analogous to using fingerprints to uniquely identify people.

This tag is intrinsic because it is formed from the surface of the controlled item. There are also attached tag concepts that require a secure bonded interface to the controlled item. An intrinsic tag has no interface, so it is much harder to transfer to an uncontrolled item than an attached tag. Furthermore, for the covert mode an intrinsic tag is much easier to make inconspicuous than an attached tag.

The plastic-casting intrinsic-surface tag is read in two steps. In the first step, the controlled-item surface is field-read by a human with a container of solvent and a strip of casting tape. For the second step, the casting is taken to a central laboratory for the SEM examination. Compared to other tag concepts, this tag is novel because the fielded reader is non-electronic. In some overt

uses, a non-electronic reader has safety advantages and lowers intelligence concerns. For some covert uses, this simple reader may also be more inconspicuous than a bulky electronic reader.

The plastic-casting intrinsic-surface tag is composed of two field elements. The primary field element is the unique intrinsic-surface topography of a small authentication area (nominally 1-cm square) on the controlled item. Plastic castings are made from the authentication area during inspections. The secondary field element is a removable bar code label which is placed over the authentication area. This label is used to assist an inspector in locating the authentication area, to provide an accounting convenience, and to protect the surface. For the covert mode the bar code label would be omitted.

This report describes both SEM and casting technologies. Numerical authentication algorithms are defined. A detailed description of the authentication process is provided. Surface duplication experiments are described. Tag authentication based upon the modulation transfer function is explained. Comments on the external adversary analysis of this tag are provided. Additional work areas to further develop the tag are outlined. The plastic-casting intrinsic-surface tag is compared to three other tagging concepts. Finally, the advantages and disadvantages of this tag are discussed.

This tagging technique is ready for limited use. However, an equipment upgrade would be needed to increase the throughput of castings, so that a practical number of castings could be authenticated.

II. CONCEPT DESCRIPTION AND PHENOMENOLOGY

A. Concept Technologies

The intrinsic-surface fingerprint tagging concept is based on two important technologies: (1) capability to make a quality casting of microscopic surface features; and (2) commercial microscope hardware and software modified for this application to make high-resolution comparison of digitized casting images. Both these technologies were well established and understood before being applied to tagging.

B. Casting Phenomenology

The intrinsic-surface, plastic-casting tag is authenticated by comparing baseline and subsequent field-inspection castings of a controlled-item surface. This tag depends upon the casting being able to capture the sub-micron scale topography of a small surface area. The topography can be enhanced to thwart duplication by forming narrow grooves in the surface with an adhesive such as sandpaper.

These castings are identical to what microscopists refer to as surface replicas. This tag builds on extensive prior experience with microscopic examination of replicas. However, in this report, the term replication is reserved for use in describing methods to attempt tag duplication (see Secs. II.D.2 and VI.A).

The particular casting technique uses a solvent-thinned, cellulose tape to make the casting. Just prior to application, the tape is dipped in acetone solvent to thin the tape. When the thinned tape is applied to the surface, a liquid layer of cellulose acetate dissolved in acetone clings to the remaining solid tape. Surface tension draws the liquid deeply into the narrow surface grooves. The cellulose-acetate solute is drawn into the grooves along with the solvent. As the solvent evaporates, the solute is left to precipitate in the grooves. Cellulose-acetate precipitate molecules cross-link to form a tough plastic that becomes part of the tape. The acetone solvent, cellulose-acetate solute approximates an optimal casting system because:

* The surface tension of acetone is very low. A low surface tension provides a high driving force that draws the solvent deeply into surface grooves. Surface tension is the driving force that causes a liquid to rise in a capillary tube partially immersed in the liquid, and the height the liquid rises in a tube is inversely proportional to the surface tension. When making castings there is no need to rely on gravity to draw solute into the grooves. Castings can be made on vertical surfaces, because acetone has such a low surface tension, that sufficient solute is drawn deeply even into upright grooves.

* The precipitated cellulose-acetate molecule is small enough to conform closely to the surface. Cellulose-acetate castings are routinely used to extract loose micro-phase particles from polished surfaces; microscopists refer to this as extractive replication. Extractive replication is successful, because the cellulose acetate solidifies to conform closely with the particles.

* The precipitated cellulose-acetate plastic is very tough and does not tear upon separation from the surface. Since each casting separates from the surface in one piece, the spatial relation between small subareas on the

surface is preserved by the casting. When two castings are compared there are no tear lines through the region of interest in either of the castings. Indeed, cellulose-acetate toughness is the reason the first casting on a newly formed tag is discarded. Loosely adherent features of the surface are broken away when the first casting is pulled off the surface. In addition, the first casting also removes debris from the sandpaper used to roughen the surface.

Some potential tag surfaces such as fiberglass may be soluble in acetone. For acetone-soluble surfaces, a water-soluble form of cellulose acetate can be used. Cellulose acetate solubility is a function of its acetyl content. The acetyl content is lower for water-soluble compared to acetone-soluble cellulose acetate. However, the surface tension of water is higher than acetone, so water-soluble acetate may not reproduce fine surface details quite as well as acetone-soluble cellulose acetate.

C. Scanning Electron Microscope (SEM) and Digital Imaging of Casting Surfaces

The SEM is used to examine castings because it provides both a high magnification and great depth-of-field compared to other microscopes. Fundamentally, an electron microscope is superior to an optical microscope because the image is formed with shorter wavelength radiation. It is useful to compare the SEM to an optical microscope for both the maximum magnification and the depth-of-field. The highest useful SEM magnification is 300,000X, while the highest useful magnification of an optical microscope is 2,000X. The optimal magnification range recommended for tag authentication is around 5,000X, so this is well within the capability of an SEM. At the same magnification, the depth-of-field of an SEM is about four hundred times that of an optical microscope. The large SEM depth-of-field results in a three-dimensional view of the microscopically rough casting surface. Using an SEM as a tag reader is technically appropriate since it is a sophisticated, highly developed, commercial instrument.

Castings are examined in the SEM in the secondary-electron imaging mode. Figure 1 is a schematic of the SEM. A collimated electron beam originates in the electron gun. The energy of the electrons used for casting examination is about 5,000 electron-volts. As the beam travels down the electron column towards the specimen, the beam diameter is reduced by a condenser lens system. Then, the beam is focussed on the specimen by the objective lens. Each beam electron excites several low energy (~1 electron volt) secondary electrons in the specimen. Most secondary electrons remain in the specimen. Because of their low energy, only secondary electrons that originate within a few nanometers of the specimen surface can escape. Therefore, escaped secondary electrons provide a signal originating near the specimen surface. These electrons are gathered by a positively biased detector. The detector signal is amplified by a video amplifier, and the amplifier output is fed to the cathode ray tube (CRT) used to view the specimen. At any instant, the CRT brightness is proportional to the secondary electron signal.

The SEM forms an image on the CRT by scanning the specimen. Within the objective lens are scanning coils that continuously raster scan the electron beam on the specimen. Both the scanning coils and the CRT deflection coils are driven by the same scanning circuits. This results in sympathetic specimen and CRT raster patterns. Moreover, the magnification is the ratio of the CRT raster length to the specimen raster scan length. Since the CRT raster length is fixed, the magnification is increased by shortening the specimen raster line. Eight raster

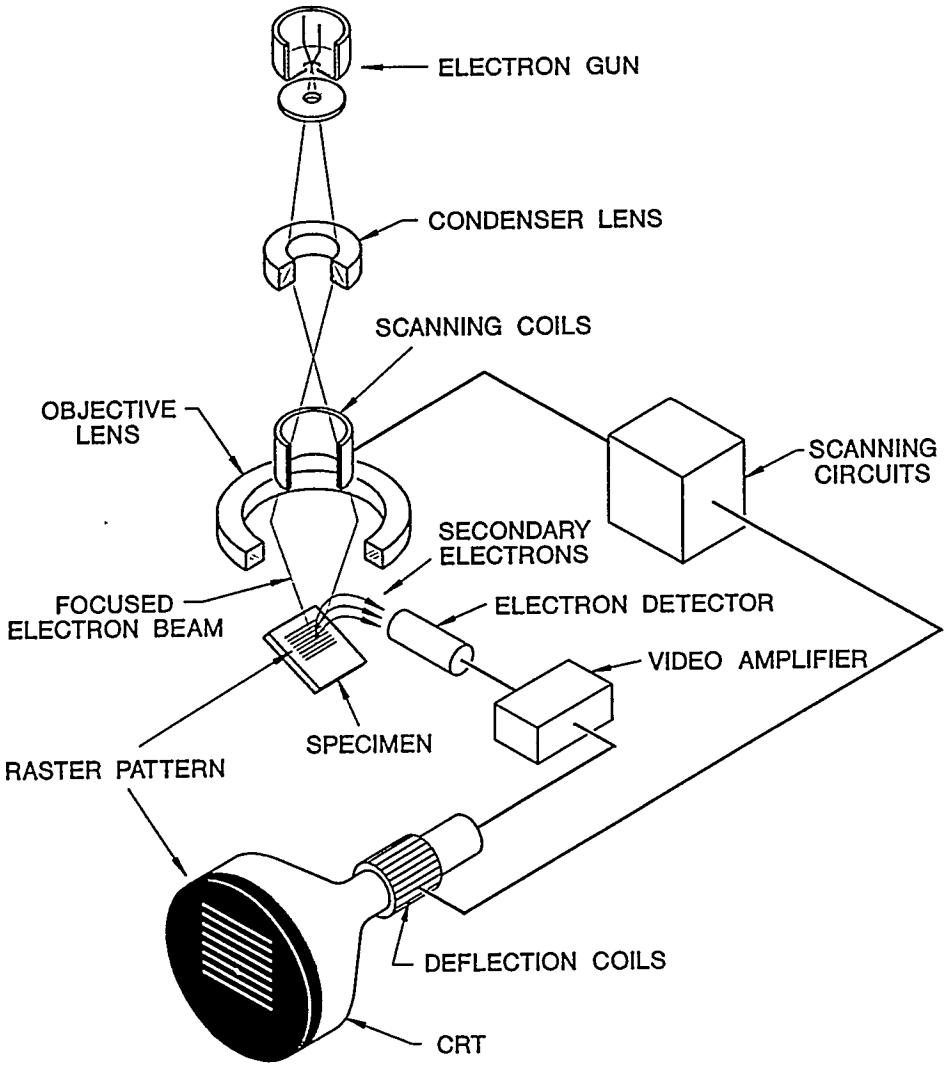

Fig. 1. Scanning Electron Microscope Schematic

scan lines on both the specimen and the CRT are schematically depicted in Fig. 1. There are 500 to 2,000 closely spaced scan lines in a typical SEM image. Because the scan lines are so close together, the image is normally free of raster artifacts.

Image contrast is established by the height of a specimen feature. As mentioned previously, local CRT brightness is proportional to the secondary-electron signal from a particular point on the specimen. Bright features on the CRT correspond to high specimen features (features closer to the objective lens), because more secondary electrons can escape from the specimen and be detected compared to low features. Contrast formation in any specimen examined at low magnification is such that an SEM image looks remarkably like an optical image. Specifically, the SEM image appears similar to an optical image formed by viewing the specimen along the electron beam axis while illuminating the specimen with a light source positioned at the secondary electron detector.

The castings are sputter coated with approximately 100 Angstroms of gold before being examined in the microscope. The primary benefit is this highly conductive gold layer drains electrons from the non-conductive casting surface. Thus, there is no charge on the casting surface that would defocus the SEM electron beam. There are two other benefits of the gold layer. The first is it protects the polymeric casting from beam damage. The second is that more imaging secondary electrons are produced in the high atomic number gold layer than in the low average atomic number casting. One potential limitation of the gold layer is that gold grain boundaries are visible at magnifications near 50,000X. However, since the castings are authenticated at 5,000X, these grain boundary artifacts are not resolved. It should be noted that castings can be examined without sputter coating in a special SEM with a field-emission-gun, electron source.

Casting authentication requires a numerical comparison of digitized casting images. The analog SEM image is converted into pixels by dividing each raster into equal-length raster subincrements. Each subincrement is recorded as an integer gray-level proportional to the average brightness. If the subincrement length is equal to the distance between raster lines, the digitized image has square pixels.

D. Signature Correlation Theory

1. Introduction to Signature Correlation

Signature correlation numerically describes how well castings compare and ultimately leads to pass-fail tag authentication criteria. The criteria for signature correlation are based upon experimental results. Specifically, they are based upon comparing castings from original surfaces and replicated surfaces. The linear correlation coefficient (LCC) is regarded as the classical statistic to compare images. While useful, the LCC is found to be deficient for this application. The LCC provides high correlations when comparing castings from the same surface. However, the LCC also provides high correlations between images of original and replicated surfaces, even though there are obvious visual differences between these images. An additional statistic called the local sum is necessary to authenticate the images. This statistic is formulated to reflect the visual differences between original and replicated surfaces. Pass-fail criteria based upon both the LCC and the local sum have been developed.

2. Replication Method

The original surface was a 1-cm diameter, 60%Au-40%Pd disk, scratched in one direction with 80-grit sandpaper. Rows of micro-indent marks were also placed on the disk to facilitate subsequent azimuthal alignment in the SEM. This replication work was reported previously [1].

The replication method is based upon standard techniques used by microscopists. Replica surfaces are made according to the steps shown in Fig. 2. The first step is to make a cellulose-acetate negative replica of the original Au-Pd surface. This negative is separated from the original surface, turned over, and sputter-coated with 500 to 1,000 nm (5,000 to 10,000 Angstroms) of gold to form a positive replica. After sputter-coating, the negative and positive are placed in a special SEM mount, so the cellulose acetate is above the gold foil. This mount has a support screen for the delicate gold foil. Then the mount is placed in acetone to dissolve the cellulose-acetate negative. After drying, the positive-replica gold-foil surface is examined in the SEM along with the original Au-Pd surface. Both the gold and the gold-palladium surfaces are essentially free of surface oxides that can degrade the ultimate resolution of the SEM. Therefore, surface features for both materials are equally well resolved.

Digital images of these surfaces were obtained at magnifications up to 5,500X. In order to obtain the best agreement between images, it was important to preserve rotational alignment between the SEM beam, specimen, and secondary-electron detector. Alignment between multiple specimens in the SEM was kept within approximately two degrees, by scribing the SEM screen with removable alignment marks at the centers of the cross patterns formed by the micro-indent marks. This rotational alignment tolerance was sufficient to obtain high image correlation between different specimens.

Because the tag is based upon casting authentication, it would have been more desirable to compare castings from originals and replicas, rather than directly comparing the originals and positive-replicas. However, the thin, positive-replica surfaces were too fragile to survive the casting process. The original surface may be considered as the zeroeth generation surface, the original casting a first generation surface, the positive-replica a second generation, and a casting from the positive-replica as a third generation surface. Therefore, the original and positive-replica comparisons were two generations apart as would be castings made from these surfaces. Because both comparisons were two generations apart, basing the signature correlation upon original versus positive-replica surfaces is a good approximation. For more discussion on the generational significance of the surfaces see Section VI.A. Castings from the original surface were also made, and digitized comparisons of these images up to 4,000X were used to determine signature correlation.

3. Linear Correlation Coefficient

a. Gray-Scale Image Registration, Image Noise, SEM Operation

Before two digital images derived from the same surface can be compared, a certain amount of processing is necessary to register them. Registration is needed to correct for small translation, magnification and rotational misalignments between the two images. These small misalignments result from the inability of the SEM operator to identically align two similar specimens with the SEM stage. For each digital image, a gray-scale value is associated with each address

STEP 1, MAKE NEGATIVE REPLICA

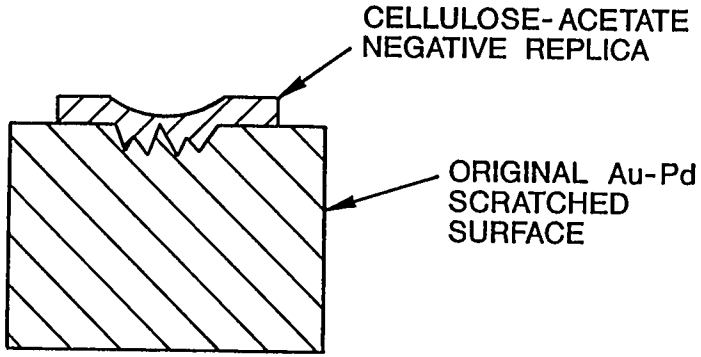

STEP2, COAT GOLD VAPOR ON NEGATIVE REPLICA

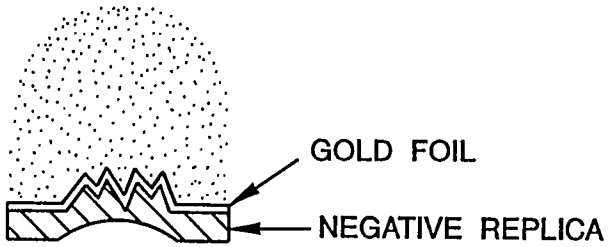

STEP 3, BACK UP GOLD FOIL

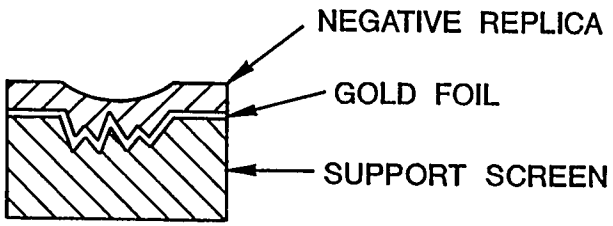

STEP 4, DISSOLVE NEGATIVE REPLICA

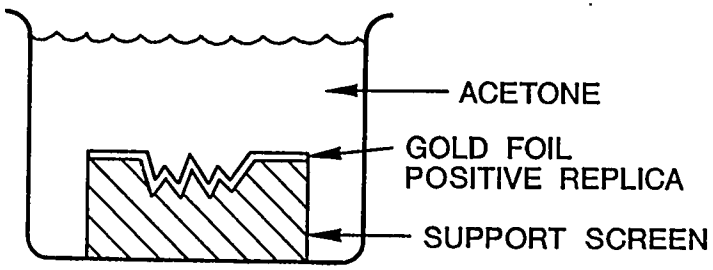

Fig. 2. Replication Method

(pixel) in the image. So for digital image A, A(x,y) is the gray-scale value of the pixel associated with each (x,y) address. In this study, each pixel had 256 possible gray-scale intensity values. To authenticate two digital images, A and B, registration is achieved when each (x,y) address of both images is for a correspondent feature on the surface(s) being compared. A classical measure of image registration, known as the linear correlation coefficient (LCC), is maximized at the optimum registration. The LCC is linear because it is invariant for a linear transformation of either or both images. If digital images A and B are linearly transformed, so their means are zero and their standard deviations are unity and N is the number of pixels in each image, the LCC is defined by Eq. (1).

$$LCC = \frac{\sum_x \sum_y A(x,y)\, B(x,y)}{N} \qquad (1)$$

Eq. (1) shows the LCC is proportional to the sum of product of the pixels in each image with the same x,y address. According to Eq. (1), both high features (pixel values > zero) and low features (pixel values < zero) contribute positively to the LCC, when the same surface feature coordinates are aligned. The maximum LCC obtained after all the registration misalignments are corrected can also be used for tag signature correlation. ANL has reported [2] on the use of correlation for treaty verification.

Theoretically, the LCC can range from one to minus one. An LCC of one indicates perfect agreement, while an LCC near zero would be expected for totally uncorrelated images from two different surfaces. Practically, the LCC is never one because of differences between surfaces, SEM noise, analog-to-digital (A/D) conversion errors, magnification misalignment, and rotational misalignment.

Details of the registration process and LCC determination as implemented by the Semper software used for this work are described in Appendix A. Semper is a high-level, image-processing language, and it is a trademark of Synoptic's Ltd., Cambridge, United Kingdom.

It is useful to obtain the LCC between two images of the same surface without moving the SEM stage. When these images are compared, differences between surfaces and both magnification and rotational misalignments are eliminated. A composite signal-to-noise (S/N) ratio from instrument noise and A/D conversion error can be calculated from this LCC according to Eq. (2).

$$S/N = |LCC|/(1-|LCC|) \qquad (2)$$

Typical values of LCC for two images of the same surface range from 0.95 to 0.98, so the S/N ratio ranges from 19.0 to 49.0 using Eq. (2). When obtaining SEM images, it is useful to use Eq. (2) to check that the S/N ratio is high enough to obtain low-noise images.

The gray-scale histogram is another important factor in attaining high LCC values. This is a plot of the population of each of the 256 possible pixel intensities. The gray-scale histogram is mainly determined by the SEM contrast and brightness settings. In order to achieve the highest LCC values, it is important to adjust contrast and brightness, so the histogram population almost spans the entire 256 gray-scale range, but diminishes to zero pixel population for gray values near zero and 255.

b. Comparison of Images Using LCC

Figures 3 and 4 compare two sets of gray-scale images. Figure 3 is a comparison of two casting images from the same original; these two images have an LCC of 0.919. Figure 4 is a comparison of an original with a replica, and these two images have an LCC of 0.875. Visual inspection shows that the images in Fig. 3 agree better than those of Fig. 4 in the brighter areas that represent high areas in the surface. However, there is only a 5% difference in the LCC, so the LCC provides only a crude authentication with limited discrimination. Note that Figs. 3 and 4 also present another image comparison statistic called the local sum. This statistic is described in a subsequent section.

Figure 5 presents another pair of images of an original and positive-replica illustrating disagreement among the brightest pixels similar to that of Fig. 4. For illustrative purposes, this image pair is repeated twice in the top half of Fig. 5. It is possible to extract rectangular subregions around the brightest areas and determine the correlation between subregions. Two sets of subregions are correlated in Fig. 5. These subregion sets are shown in the lower part of this figure, and the sources of the subregions are marked in the top part. Figure 5 shows that the broad subregion shown in the lower left of the figure has a LCC of 0.828, only 0.5% less than the LCC of 0.832 for the whole image comparison. In the lower right is a very narrow subregion set; it had a low LCC of 0.414. Therefore, visual observation of the disagreement is confirmed by the LCC if small enough subregions near the bright areas can be chosen for correlation. However, choosing and correlating all such small subregions in the two images being compared is a difficult process to implement.

From examining Figs. 3, 4, and 5, it is apparent the LCCs calculated from the whole images are a rather insensitive indicator of image disagreement. A more sensitive and simple means to authenticate an image based upon its brightest areas was formulated.

4. Binary Images and Local-Sum Comparison

Because the differences in the gray-scale images were clustered near the brightest pixels, it is necessary to emphasize the brightest pixels before comparing the images. A standard image-analysis technique used to emphasize features with a common gray-scale intensity range is to form a thresholded binary image from the gray-scale image. Each pixel in the binary image is set to one if the corresponding pixel in the gray-scale image falls in the intensity range of interest. Otherwise, the binary pixel is set to zero. For the local-sum method, each binary-image pixel value is set to one if the corresponding gray-scale pixel is in the brightest 15% of pixels. In this manner, the brightness-thresholded binary images A_b and B_b are derived from their respective gray-scale brightness images A and B. A_b and B_b can be compared to determine a numerical score for comparison. Inspection of Fig. 5 shows the replica bright subregions to be wavy and discontinuous compared to the original bright subregions. Therefore, the brightness-threshold process visually captures the differences between the original and replica. Appendix A provides a more detailed description of the binary image processing and its implementation with the Semper software.

A simple way to compare the binary images is to form the absolute-difference image C_b from A_b and B_b according to Eq. (3).

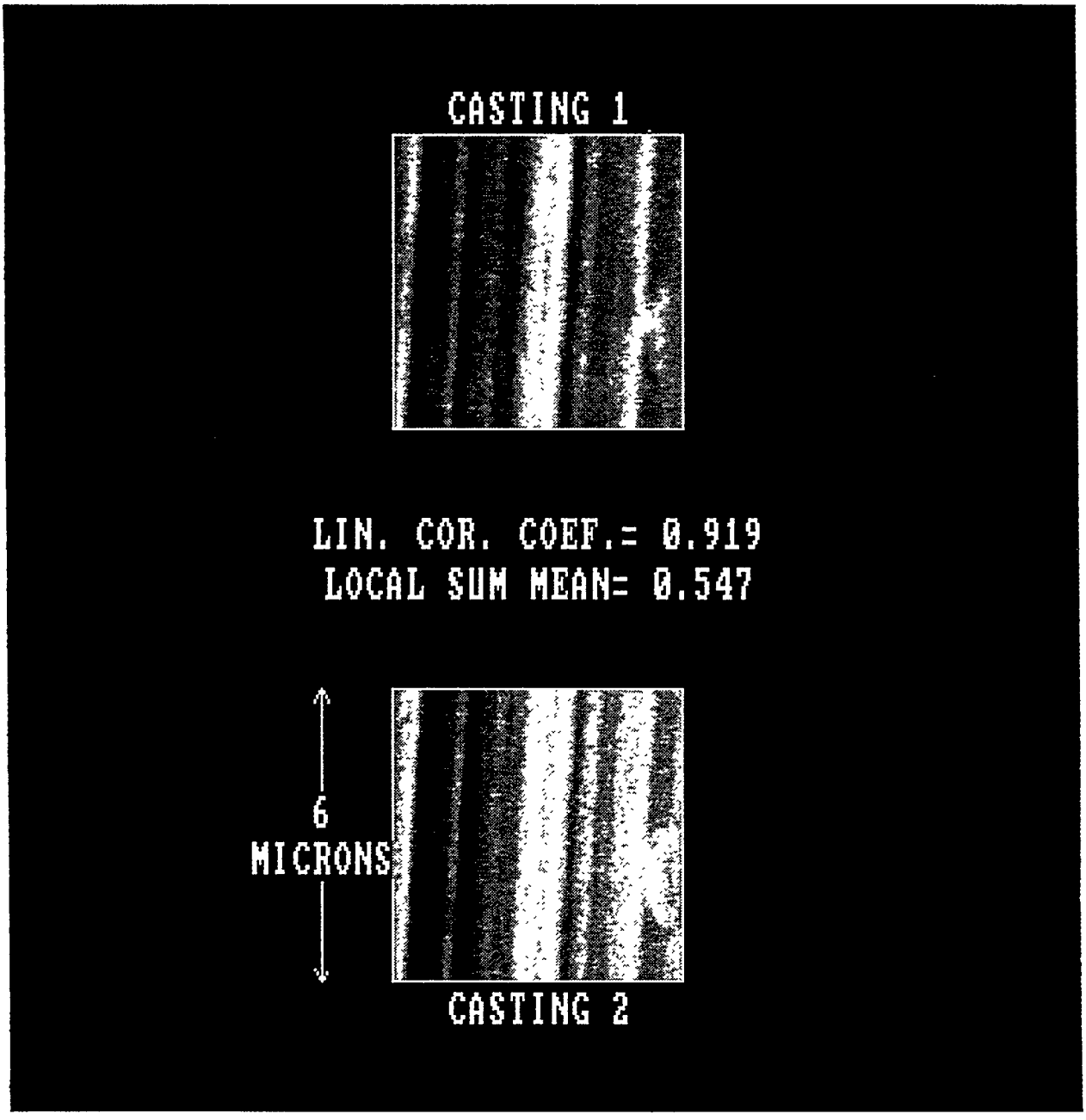

Fig. 3. Casting Image Comparison Using Linear Correlation Coefficient and Local-Sum Mean

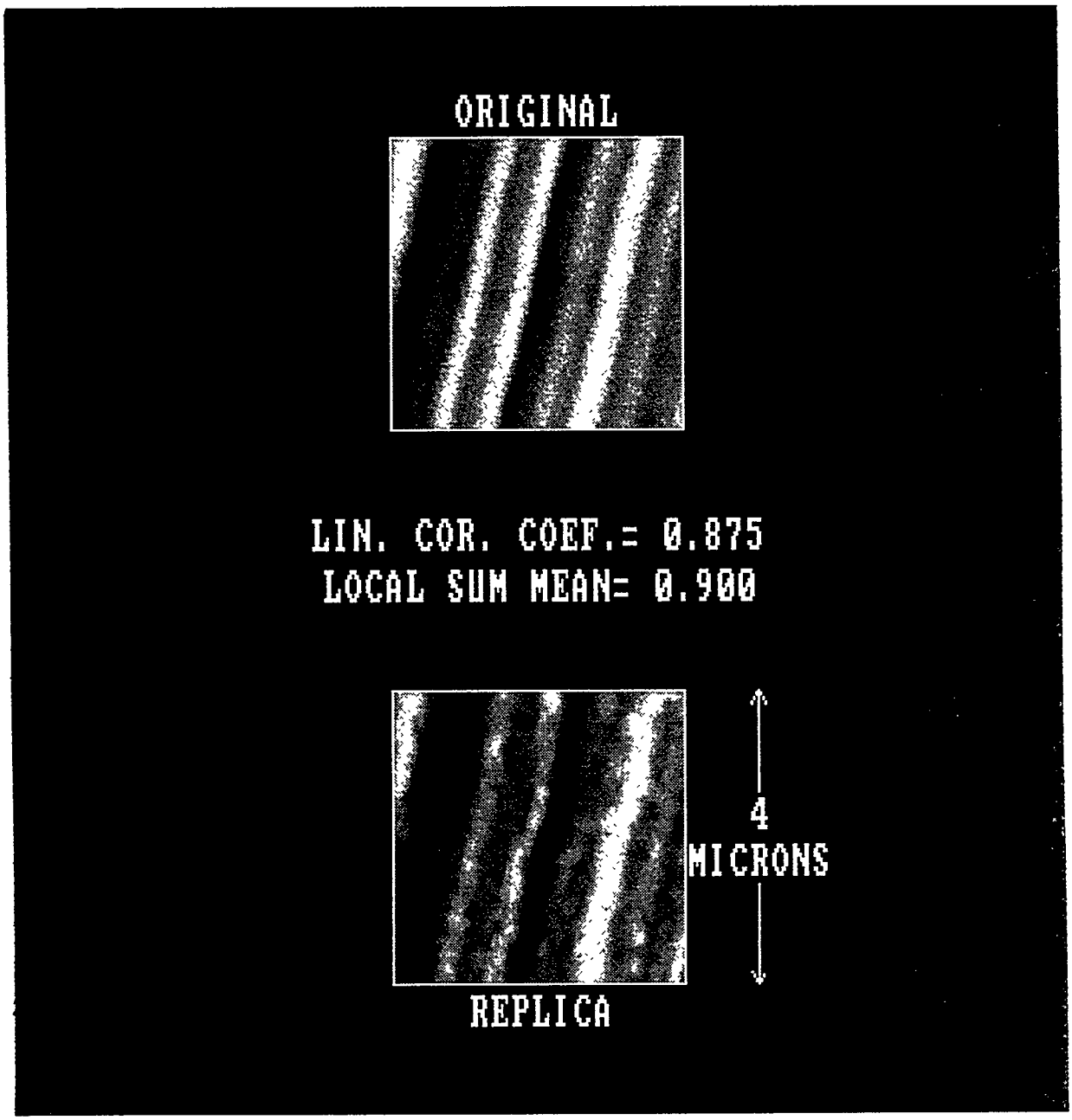

Fig. 4. Original-Replica Image Comparison Using Linear Correlation Coefficient and Local-Sum Mean

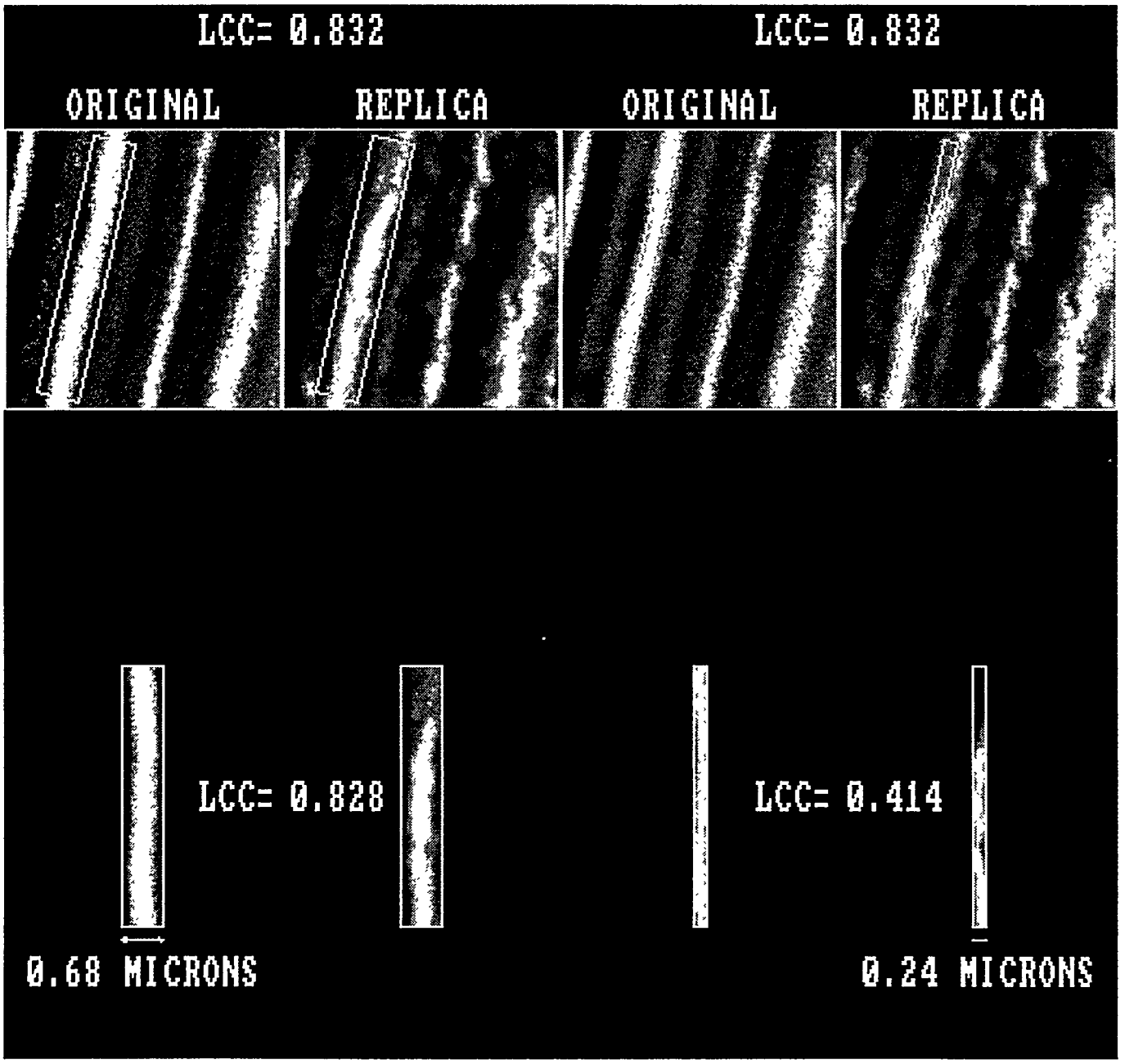

Fig. 5. Linear Correlation Coefficient for Subregions Around Bright Areas

$$C_b(x,y) = |A_b(x,y) - B_b(x,y)| \quad (3)$$

The pixels in image C_b are set to one for the pixels in A_b and B_b that disagree. Otherwise the pixels are set to zero. Therefore, image C_b gives a binary indication of the pixels in A_b and B_b that disagree. A possible tag acceptance criterion derived from C_b is simply its mean. Low means indicate good agreement. The mean of C_b can span from zero (perfect agreement) to 0.3 (complete disagreement for 15% threshold).

Another way to view C_b is to form a local-sum image. This local-sum image also presents a gray-scale rendition of the local disagreement between images A_b and B_b. The local-sum image, referred to as image D, renders the degree of disagreement of local p by p pixel clusters in C_b. Each local-sum pixel D(x,y) is produced by summing each pixel $C_b(x,y)$ with its p^2-1 nearest neighbors and placing the sum in D(x,y). The pixels within a distance p-2 of the border of C_b can't be summed over p^2 pixels. Therefore, if the image C_b has dimensions M by N, the local-sum image has dimensions M-p+1 by N-p+1. The pixel values of the local-sum image can span the range from 0 (complete agreement) to p^2 (complete disagreement). For the local sum results in this study, p is equal to 3.

Figure 6 illustrates the binary images for two castings of the same original surface. Inspection of Fig. 6 shows the binary images to be similar. This similarity results in a low value of the local-sum mean. The local-sum mean for this original-replica comparison is 0.547.

Figure 7 shows the local-sum image formed by an original and a replica and derived from the absolute difference binary image discussed previously. High means indicate poor agreement. The local-sum mean for this original-replica comparison is 0.900.

Figures 6 and 7, respectively, compare the same original-casting versus original-casting and original versus replica image pairs in Figs. 3 and 4. The LCCs for these image pairs differ by only 5%, but the local sum means differ by 64%. Therefore, the local sum mean is a better discriminator of the bright ridge-line defects in the replica image, but not present in images of two castings from the same original.

The local sum, based upon the binary images, is dependent upon the threshold limit used to derive the binary images. A brightness threshold limit of 15% was empirically determined to provide the best quantitative discrimination between original and replica surfaces.

It can be shown that the absolute-difference image mean is one-ninth the local-sum image mean for a p=3 local-sum image. Thus, the local sum renders a gray scale of agreement between two images, but does not provide numerical discrimination beyond that provided by the absolute-difference image. In other words, the local-sum mean can be more simply computed as nine times the mean of the absolute-difference image. Indeed, there is an advantage to this computation since all the pixels on the border of the absolute difference image contribute to the signature. Since the mean of the absolute-difference image can range from 0.0 to 0.3, the local-sum image range is 0.0 to 2.7.

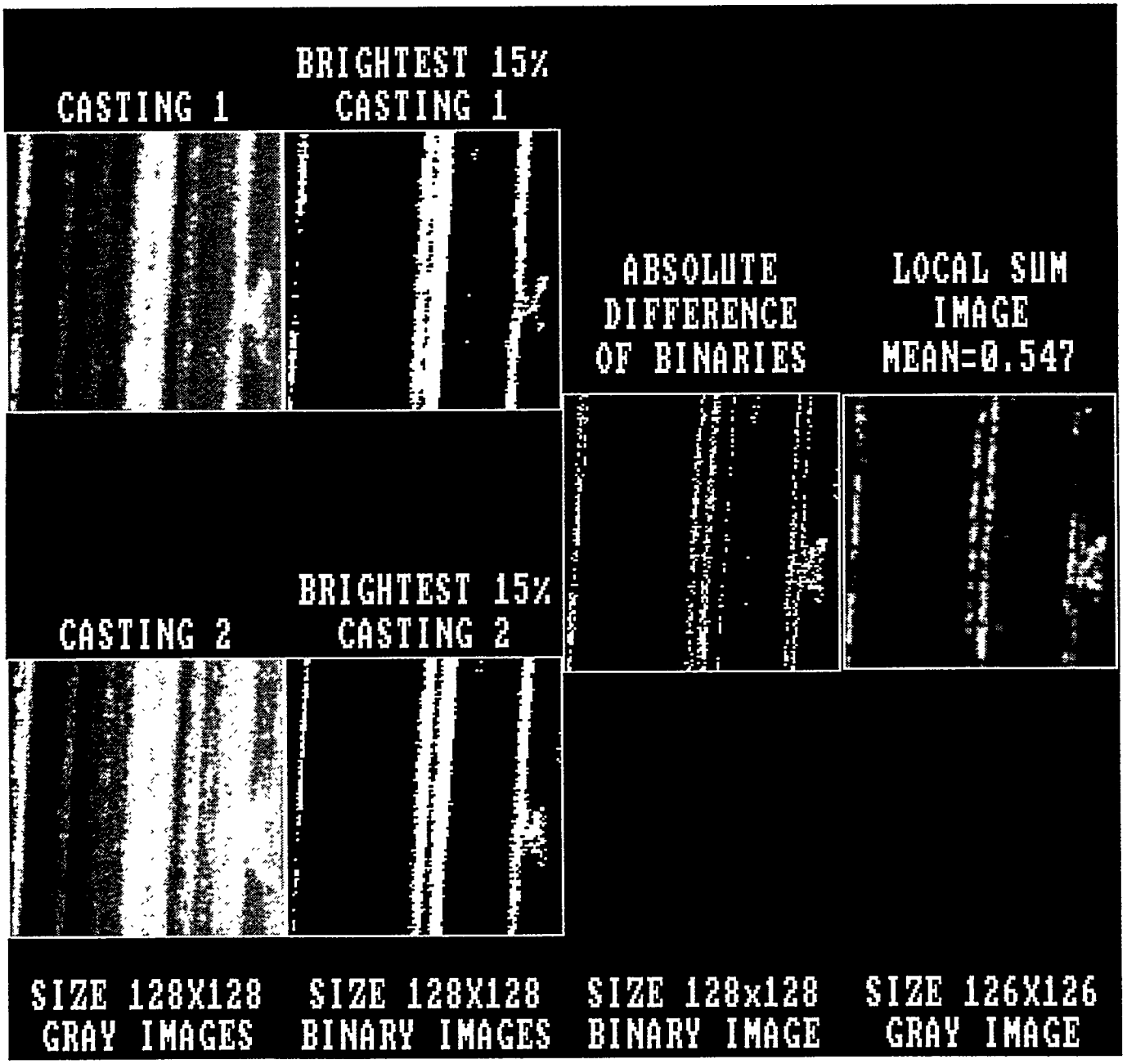

Fig. 6. Illustration of Steps in Calculating the Local-Sum Image for Figure 3 Gray-Scale Images

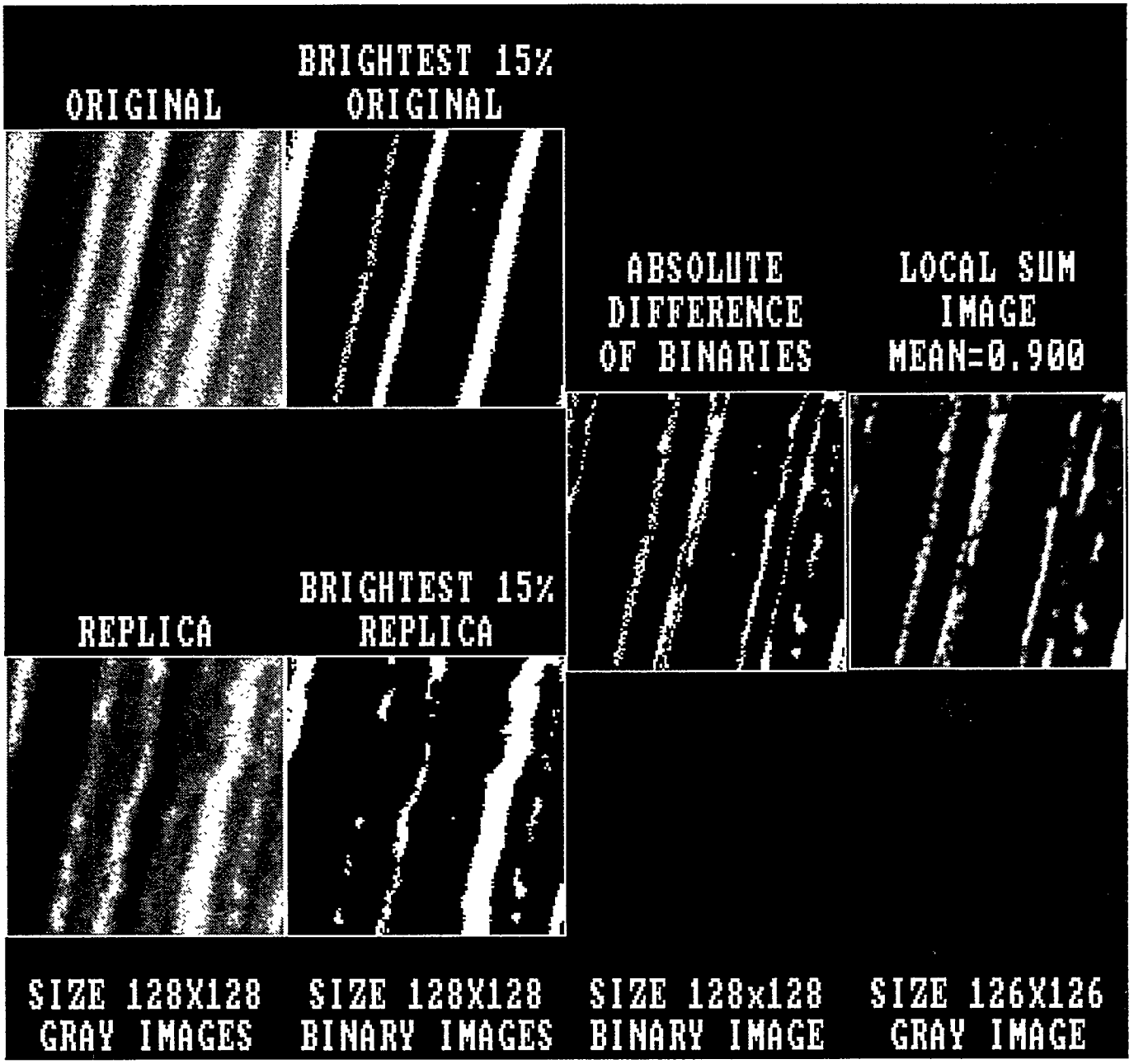

Fig. 7. Illustration of Steps in Calculating the Local-Sum Image for Figure 4 Gray-Scale Images

5. Tentative Acceptance Criteria for Subareas

Table 1 presents LCC and local-sum mean values for the two types of image comparisons used to formulate the empirical acceptance criteria. The first kind of image comparison is for two castings taken from the same original surface. An acceptance criterion was formulated, so the casting image comparisons had passing scores for castings acquired at a SEM magnification of 4,000X. A second kind of image comparison related original tags with positive-replicas of the original. The acceptance criterion was formulated, so six out of seven original versus positive-replica image comparisons at 5,500X failed to meet it.

Based upon the images examined for this study, an empirical acceptance criterion is proposed. Subarea images are accepted as genuine if the LCC > 0.7 and the local-sum mean is < 0.6. Since the image-registration process computes the LCC to determine the best registration of the two images, it is determined before the local-sum mean. Therefore, if the LCC of a subarea is < 0.7, the subarea fails to pass, and the local-sum mean need not be calculated. Figures 3 and 4 show that it is relatively easy to satisfy the LCC part of the acceptance criteria. However, meeting the local-sum criteria is more demanding; only two images with their brightest pixels in registration can satisfy it.

One additional acceptance criterion must be developed as more data are examined. A 128 by 128 pixel subarea at 5,500X such as in Fig. 4 represents only 0.000016% of the 1 cm^2 tag area, so it is not feasible to investigate all the subareas in a tag. This additional criterion would determine both the percentage of subarea passes and the number of subareas that must be evaluated. An example of an overall pass/fail criterion would be to accept the surface as genuine if 80% of the subareas passed out of 144 subareas examined. This acceptance criterion will be determined from a future authentication exercise that compares castings made from original and positive-replica surfaces.

Image comparisons at lower magnifications are also presented in Table 1. These comparisons were not used to formulate the acceptance criteria, but are referred to in Section VI.A.2.a in a discussion emphasizing the importance of using the proper SEM magnification for tag authentication.

Figure 8 shows the results of three attempts to replicate the same surface. All the attempts failed to meet the acceptance criteria. Only one of these replication attempts passed the LCC part of the acceptance criteria. For this set of replicas, the LCC and the local-sum mean varied inversely. More work needs to be done to determine if this inverse relationship holds for large numbers of original-replica comparisons.

E. Application Scenario

The purpose of this section is describe the procedure, materials, and equipment used in the intrinsic-surface, plastic-casting method. This intrinsic identifier is formed from a small surface area. Location of this area is specified by protocol. The unique feature is the micro-scale topography of this surface. Baseline and subsequent field-inspection plastic castings are made to capture the micro-topography. These castings are made by inspectors at the field location, and taken to a central laboratory for authentication. A numerical indication of authenticity is obtained by comparing digitized SEM casting-images.

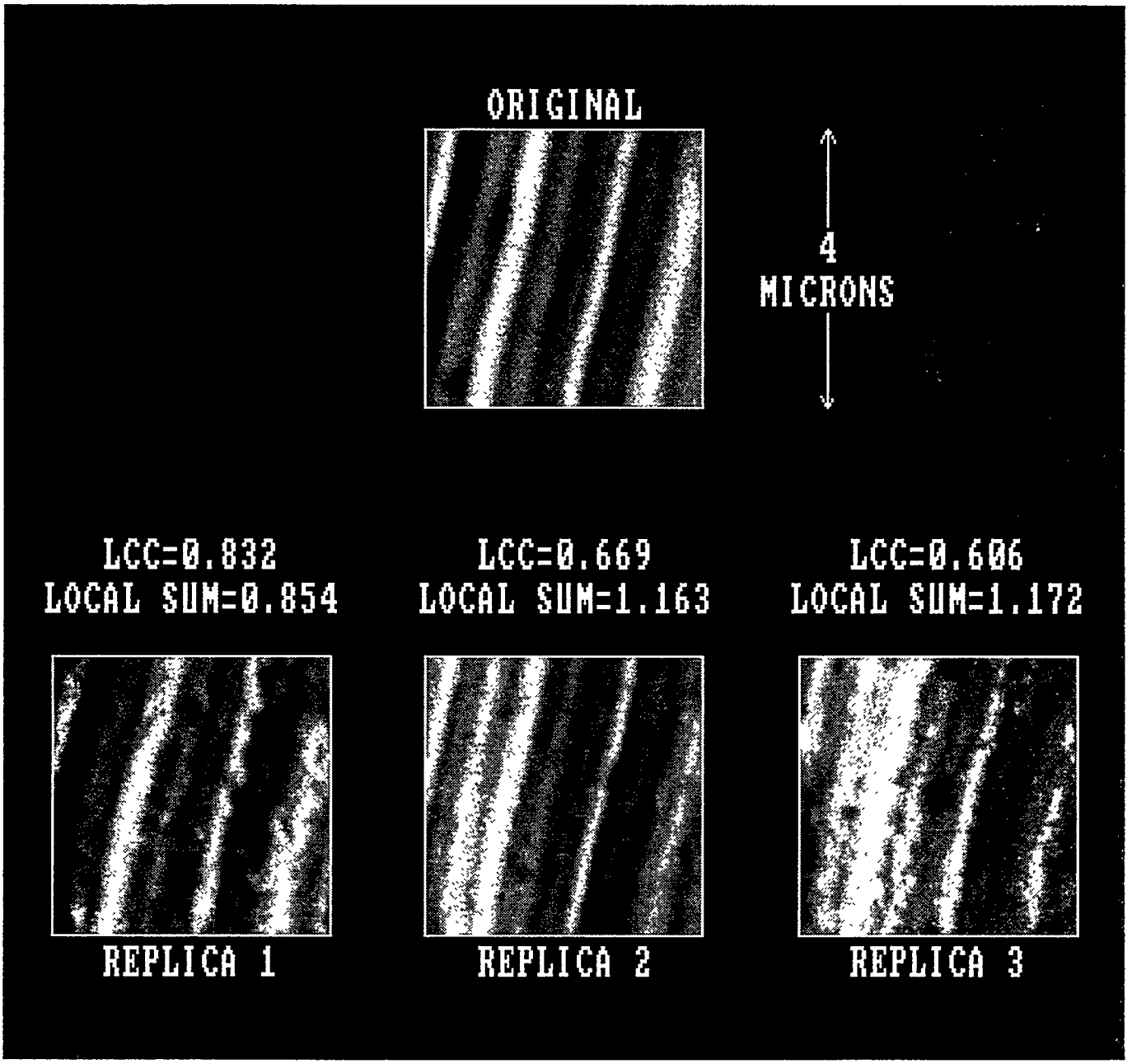

Fig. 8. Comparison of an Original and Three Replicas

Table 1				
Numerical Image Comparison Results				
Image #1 file number	Image #2 file number	Magnification	Linear correlation coefficient	Mean, local-sum image
5242ca	5241ca	4000	0.907	0.571
5244ca	5243ca	4000	0.919	0.547
5225ca	5226ca	2000	0.869	0.566
5221ca	5222ca	2000	0.895	0.451
5223ca	5224ca	2000	0.757	0.795
5227ca	5228ca	2000	0.915	0.598
5201ca	5202ca	700	0.922	0.407
5111or	5112rp	5500	0.875	0.900
5121pr	5122rp	5500	0.881	0.947
5165or	5168rp	5500	0.756	1.154
5155or	5158rp	5500	0.918	0.565
5101or	5102rp	5500	0.832	0.854
5101or	5103rp	5500	0.606	1.172
5101or	5104rp	5500	0.669	1.163
5193or	5194rp	700	0.898	0.410
5193or	5195rp	700	0.898	0.408

ca = casting; or = original; rp = replica

1. Field Procedure

a. Baseline Inspection

Figure 9 shows a six-panel sequence depicting the baseline-inspection tagging procedure. The first panel depicts a painted surface of a controlled item before tagging. In the second panel the paint has been wire brushed to expose the base metal. Not shown in the second panel is solvent cleaning of the surface. The TLI surface is marked in the third panel. First, the surface is scratched in one direction with 100-grit sandpaper to create substantial micron-scale surface topography. Then, a 0.5 to 1.0 cm authentication square is marked in the scratched area with a diamond-point scribing tool. This square helps the inspector locate the exact authentication area. The fourth panel shows a casting being made over the authentication square. Note that the casting is bar coded for identification. The first casting is discarded since it cleans the surface of sandpaper micro-debris and loosely-adherent base metal. Then, as many castings as dictated by protocol requirements are made. Panel five shows a bar-code label placed over the authentication square. The bar-code label protects the surface from environmental attack, and provides an automated inventory interface to the controlled item database. The label is attached with high-performance adhesive. Panel five shows an option with the label attached by rivets and adhesive. Finally, panel six shows the item repainted around the bar-code label.

In most applications the casting and protective bar-code labels would be scanned at appropriate points in the inspection with a bar-code reader-computer. Figure 10 shows a replica of a Laser-Wand bar code reader-computer from Hand Held Products, Charlotte, North Carolina. Inspection information can be loaded into the Laser-Wand memory before inspections. The contents of the memory can also be uploaded to the database computer after the inspection. The reader is a stand-off device that reads the bar code by scanning a laser beam across it.

In a few applications, such as tagging nuclear warheads, an electromechanical device may not be allowed in the vicinity of the controlled item. For these applications, the laser wand would not be used. The inspectors would write the bar-code alphanumerics on inspection forms.

b. Subsequent Field Inspections

In subsequent field inspections, the protective bar-code label would be removed first. Then, as many castings as dictated by protocol are made. Finally, a new protective label would be installed.

c. Making Castings

The casting material is cellulose acetate in the form of short tape strips. The particular cellulose acetate used is 5-mils thick and 1-in. wide. It is supplied as a tightly wound 6-ft-long roll by E. F. Fullam Co., Latham, New York. Strips of the tape about three inches long are cut from the roll. Bar-code labels are placed on each strip for identification as shown in Fig. 11a. Figure 11b shows a strip being dipped in acetone solvent prior to being applied. Because the tape is tightly wound on the supply roll, the strips are curled. This curl is observed, as the solvent thins the tape. When the tape is thin enough to be applied, the curl has almost disappeared. Then the tape is draped on the surface.

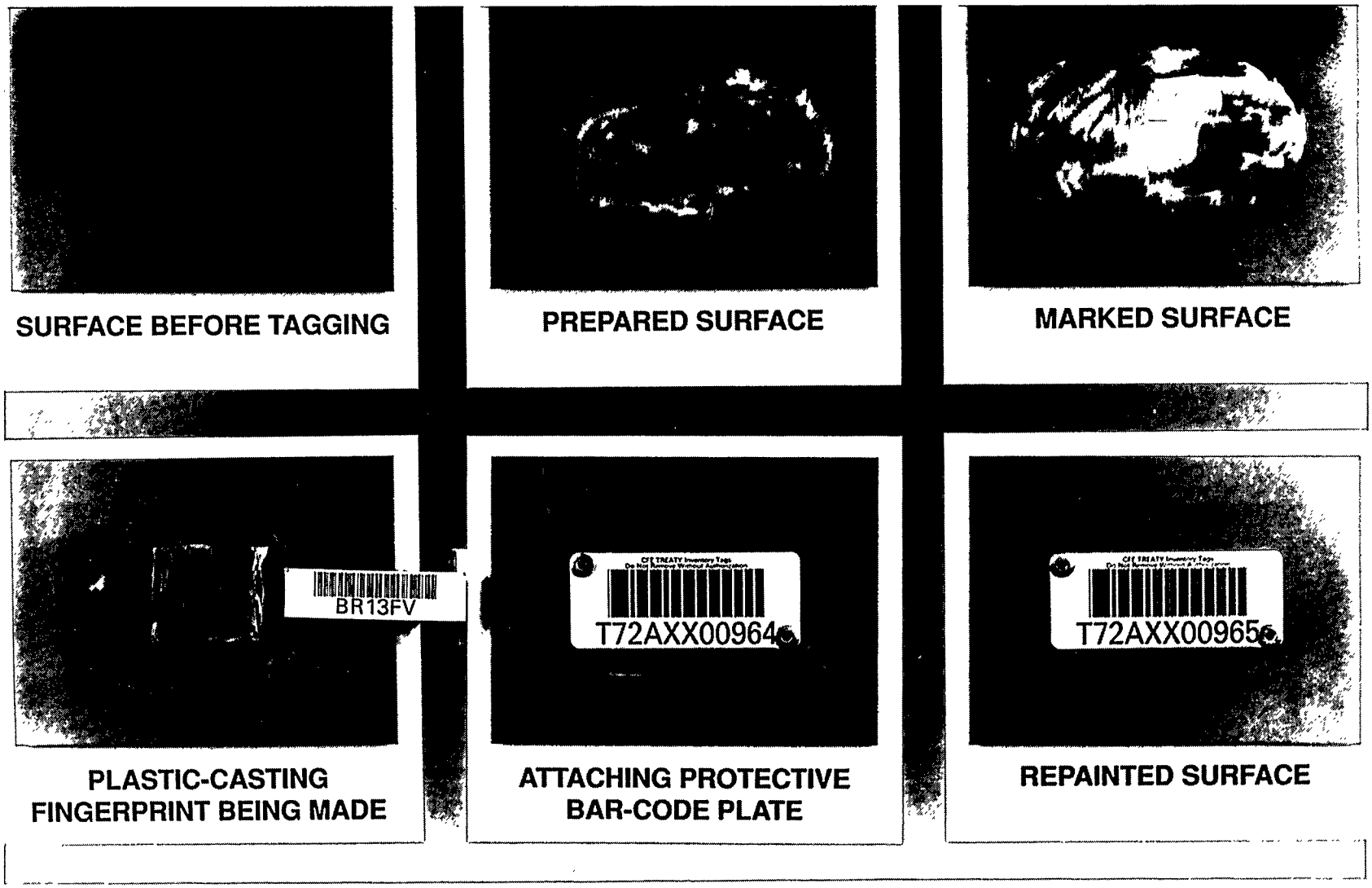

Fig. 9. Baseline Tagging Procedure

Fig. 10. Combination Standoff Bar-Code Reader and Computer (Laser Wand from Hand-Held Products)

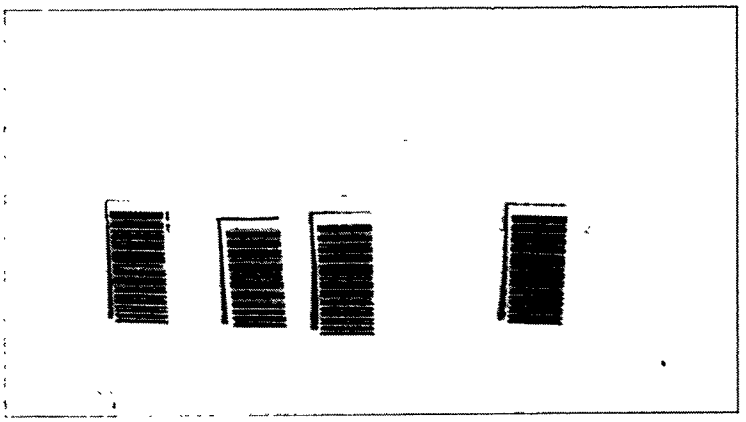

(a)

(b)

Fig. 11. Cellulose Acetate Castings: (a) Four Bar-Code Identified Casting Strips; (b) Strip Thinning Just Prior to Application on Controlled Item

There are three important details that help ensure a high quality casting:

* The tape is applied, so the remaining curl is concave as the tape is viewed from the surface.

* Draping is along the direction of the sandpaper scratches.

* The tape is draped slowly enough, so a straight tape to surface contact-line is maintained during application.

Tape concavity, draping direction, and slow draping ensure a continuous process that pushes air out of the scratches ahead of the line contact with the surface. Removal of air is necessary to minimize casting micro-bubble defects. This process is moderately tolerant to imperfections such as micro-bubbles in the casting, because only a small bubble-free portion of the casting surface is used for authentication. At ambient temperature the casting dries in fifteen to thirty minutes, and can then be peeled away from the surface if it hasn't already separated by itself. The drying process can be accelerated by heating the surface. Castings can be made on horizontal to nearly vertical surfaces.

2. Central Laboratory Procedures

a. Mount Castings on SEM Sample Stubs

The first laboratory operation is to mount the casting on small aluminum or brass cylinders referred to as sample stubs. These stubs allow easy handling, precise SEM stage positioning, and simplified long-term storage. First, the casting bar code is read and associated with an identification marked on the bottom of the stub. Then, the casting is trimmed with scissors, so only the area around the authentication square remains. This trimmed casting is attached to the top of the sample stub with double-backed tape. All items that go into the microscope must be cleaned in solvent and not touched afterward by ungloved hands. Even a minute amount of grease from clean fingers degrades the SEM vacuum, and can contaminate samples.

b. Sputter Coat Castings

The stub mounted castings are coated with approximately 100 Angstroms of gold in a sputter coater. Figure 12 shows four stubs being loaded onto the sputter-coater vacuum-chamber bottom plate. Figure 13 shows the sputter-coater vacuum chamber as assembled and ready for pump-down and sputtering. This sputter coater is a Hummer VII from Anatech Ltd. of Alexandria, Virginia. The purpose of coating the castings is to provide SEM beam electrons a low-resistance path to ground. If this path is not provided, electron charge accumulates on the non-conductive tape surface. This charge would defocus the SEM beam and result in poor SEM resolution.

c. Load Castings in Stub Holder and Load Holder in SEM

The sputter coated stubs are loaded into a holder, which accepts multiple stubs. The purpose of the holder is to facilitate changing samples, as the bottom of the stub holder slip fits onto the top plate of the SEM stage. Figure 14 shows a holder with four stubs being positioned on the top plate of the stage. After the holder is mounted on the stage, the stage drawer is pushed back into the sample chamber, and the SEM is ready for pump-down.

Fig. 12. Four Stub Mounted Castings Being Loaded into Sputter-Coater Bottom Plate

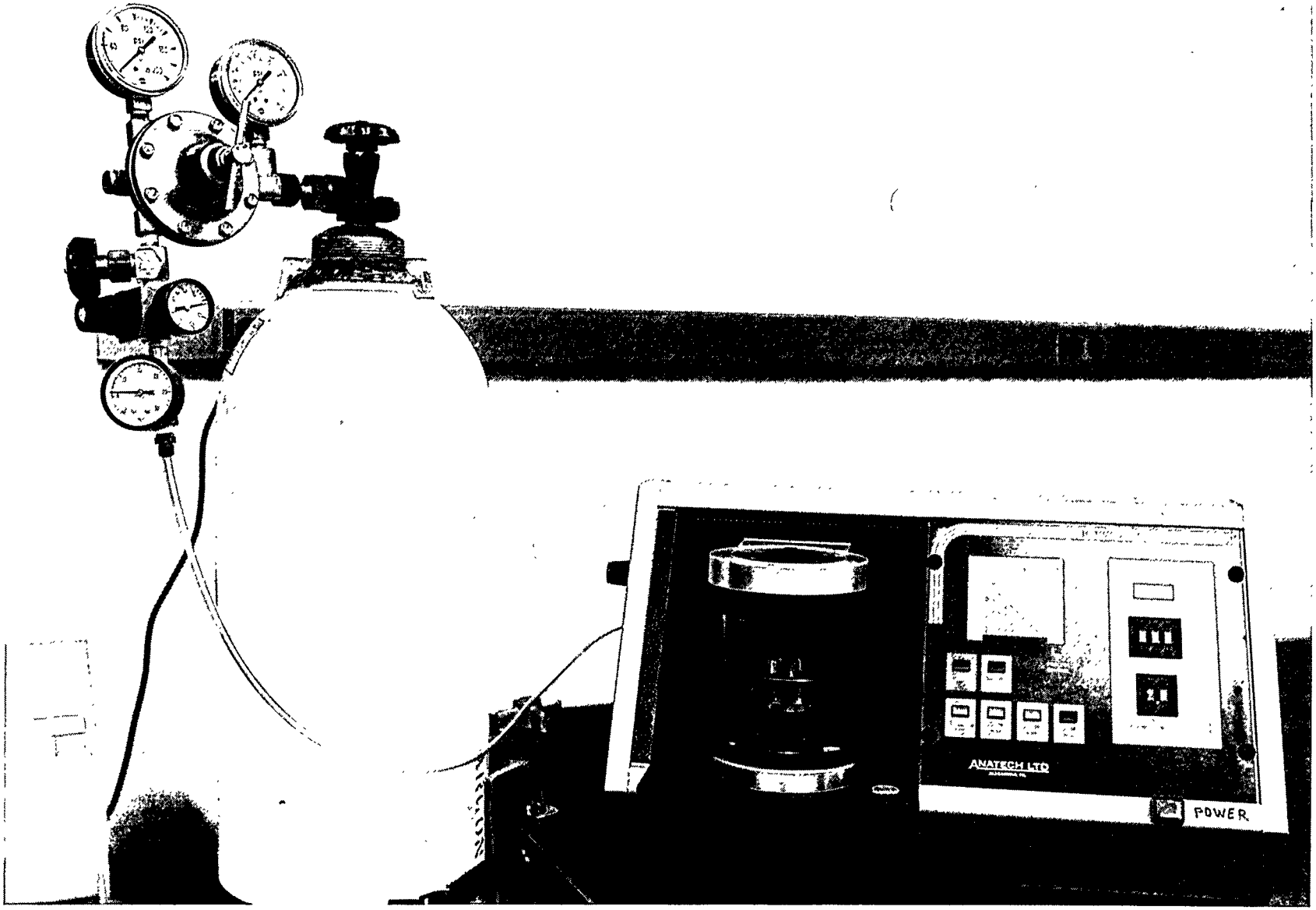

Fig. 13. Sputter Coater with Stubs Inside Vacuum Chamber

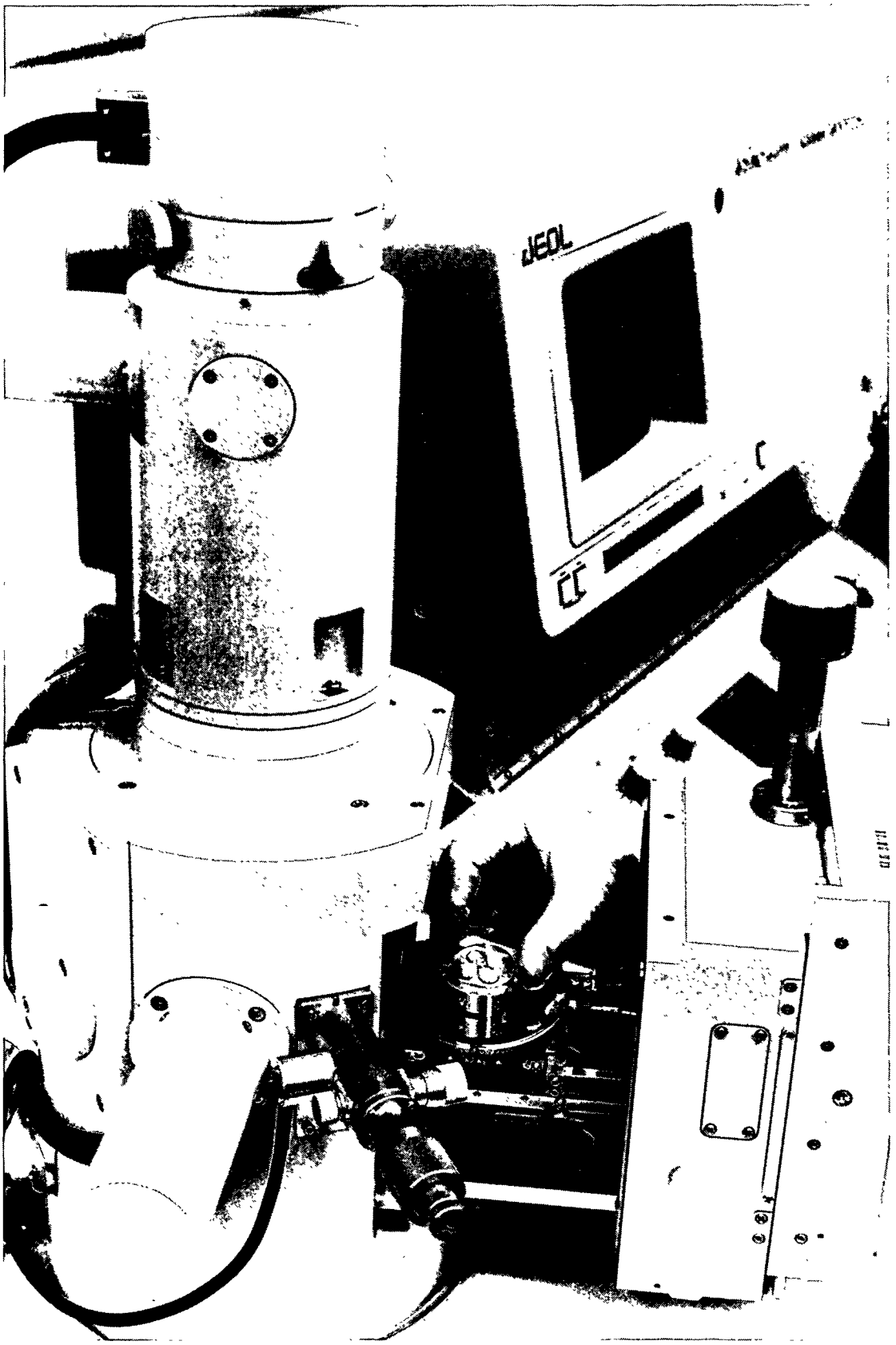

Fig. 14. Positioning Stub Holder on Top Plate of SEM Stage

d. SEM Examination

Figure 15 shows the SEM. It is a JSM 5300 from JEOL USA, Peabody, Massachusetts. The electron column is on the left along with controls that move the stage. In the lower middle is the control console. Functions such as focusing, magnification, image brightness and contrast, and astigmatism correction are performed at the control console. Above the control console is the viewing cathode-ray tube (CRT).

e. Image Digitization

The analog SEM casting images are noise filtered and digitized by a Pixie-8 frame-store from Deben Research Ltd., Ipswich, U.K. A Pixie-8, PC interface card transfers the digital image from the Pixie-8 into a PC-based image-processing system shown in Fig. 16. The system is a Quantimet 520 from Leica Cambridge Ltd., Cambridge. U.K.

f. Alternate SEM Imaging System

The JSM 5300 SEM, Pixie-8 image digitizer, and the Quantimet 520 image processing system discussed above resides in the dedicated casting authentication laboratory at Argonne National Laboratory (ANL). Recently, an improved system at ANL has been used to examine castings. The benefit of the improved system is that the digitized image has very low distortion. Low distortion allows for greater tolerance in the SEM stage positioning of the field-inspection casting. The improved system consists of a JOEL, JSM 5400 SEM and a Noran, Series II image digitizer/image processing system.

g. Authentication

Semper 6 PC image-processing software from Synoptics Ltd., Cambridge, U.K. is used to numerically compare the digital baseline and field-inspection images to determine authenticity.

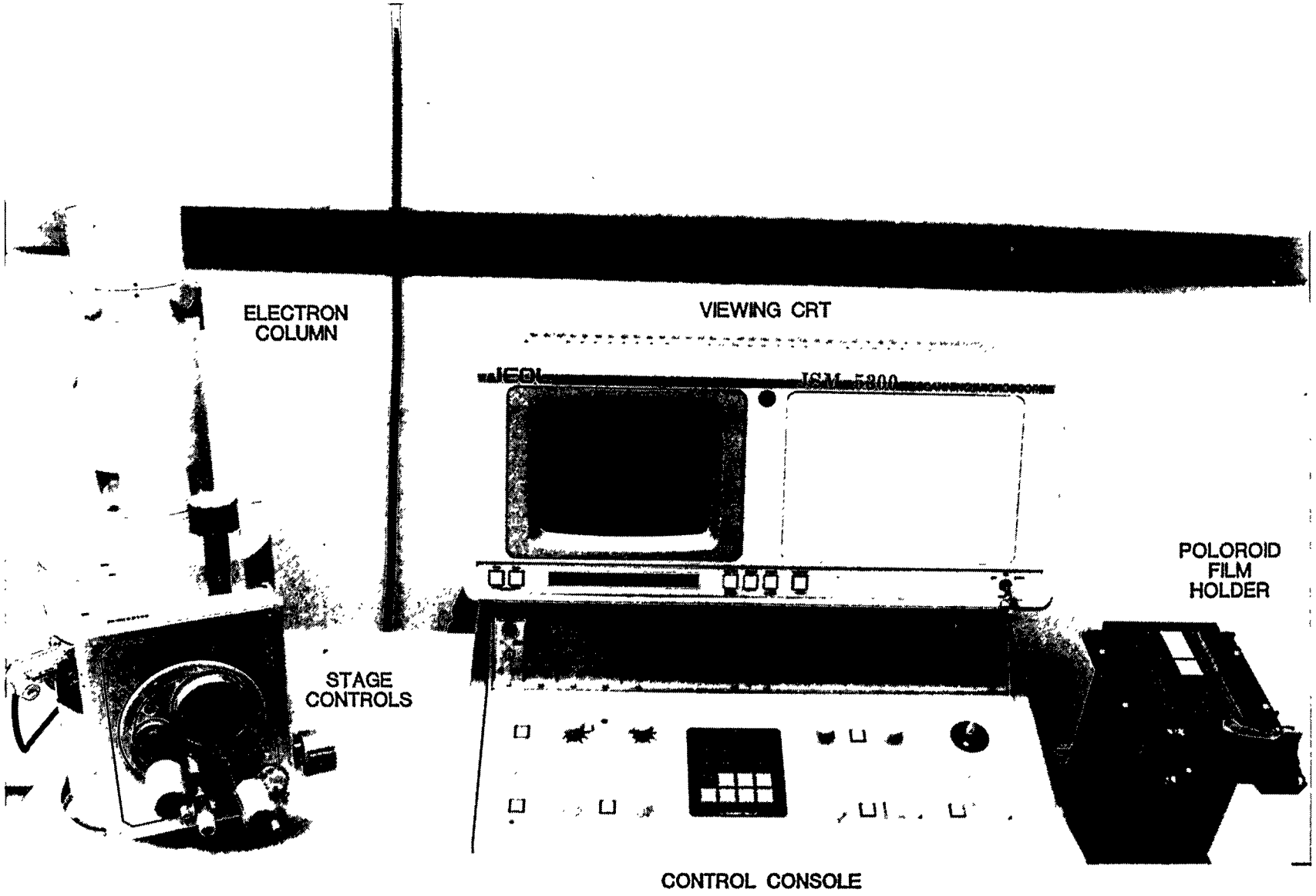

Fig. 15. Scanning Electron Microscope

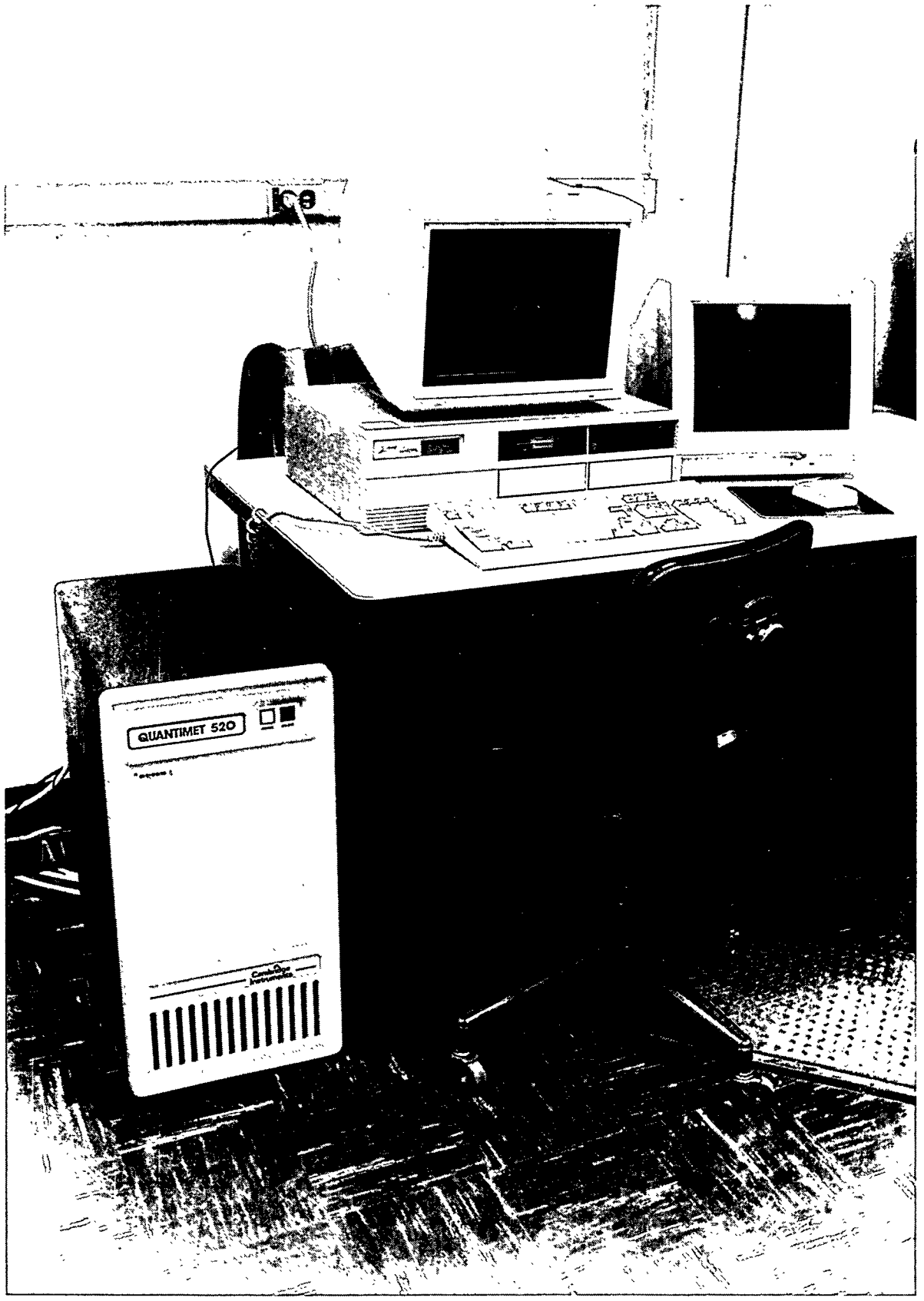

Fig. 16. PC-Based Image Processing System for Numerical Authentication of Casting Images

III. PROTOTYPE SYSTEM DESCRIPTION AND DESIGN

All prototype equipment and software are commercially available. Use of this equipment and software in an application scenario is described in Section II.E. The software is described further in Appendix A. A list of commercial vendors is provided in Appendix B.

IV. PROTOTYPE OPERATION

The sequence of use of the commercial equipment and software is described in Section II.E. All of the commercial equipment and software have comprehensive vendor-supplied documentation such as operating manuals, maintenance manuals, and software guides. This documentation is available for inspection at Argonne National Laboratory in its dedicated intrinsic-surface authentication laboratory.

V. ENVIRONMENTAL TESTING RESULTS

A. Environmental Tests

No controlled environmental tests have been performed. Reference 3 is a generic assessment performed for applications involving aluminum-alloy surfaces. This reference describes corrosion chemistry and surface protection schemes.

B. Environmental Assessment

Since the intrinsic-surface identification method depends on the preservation of micron-scale surface features, it is important that the surface be preserved and not environmentally degraded. For most applications, the adhesive-bonded, bar code label (see Fig. 9, Section II.E) is sufficient to protect the tag surface.

Three important factors determine the amount of environmental protection needed: the surface material, service location, and necessary lifetime. Typical identifier surfaces are metals and composites. Metal corrosion is an electrochemical process requiring water and electrolytes to proceed. Composite surfaces such as graphite-epoxy degrade by weathering. Weathering is an ultraviolet light attack on the organic bonding in the epoxy. Preventing metal contact with either water or electrolytes, or absorbing ultraviolet before it shines on the composite is sufficient to protect the surface. Obviously, an indoor service location would eliminate both corrosive acid rain and ultraviolet attack on the tag. Similarly, a short service life limits surface attack. An example of a potential application with protected location is nuclear-warhead accountability.

For outdoor surfaces requiring adhesive-bonded, bar-code label surface protection, the surface material is important in two respects. First, the adhesive in the label must be tailored to the surface material. High energy surfaces such as metals require different adhesives than low energy surfaces such as graphite-epoxies. Second, individual metals are sensitive to specific atmospheric pollutants, and certain metals can have their corrosion resistance enhanced by specific treatments. For example, aluminum corrosion is sensitive to the sulfur-bearing, pollutant-gases SO_2 and H_2S. The natural protective oxide layer that forms instantly on any fresh aluminum surface can, if necessary, be chemically thickened to provide increased corrosion protection, as described in Ref. 3.

In summary, schemes exist to provide the necessary degree of surface protection from environmental degradation. These schemes must be tested in a formal testing program supervised by personnel with established expertise in corrosion and weathering phenomena.

VI. ADVERSARY ANALYSIS SUMMARY

A. Internal Testing and Analysis

1. Theoretical Analysis of Reliable Authentication and Discrimination Against Counterfeits

a. Introduction to the Modulation Transfer Function

A theoretical analysis of the counterfeiting vulnerability for this authentication method is presented. This analysis is consistent with the replication experiments described in Sec. II.D as well as other experimental results discussed following the theoretical analysis.

The modulation transfer function (MTF) provides a first-principle theoretical framework for analyzing intrinsic surface, plastic-casting authentication. A wide variety of imaging-system components and whole imaging systems use the MTF to analyze imaging accuracy. For example, components such as particular film types or lens designs have an MTF associated with each component. A camera is an example of an imaging system with an MTF determined by its lens and film MTFs.

Authentication by SEM images of plastic castings also relies upon an imaging system. An original controlled item surface is imaged by a system with two components. These components are the plastic casting and the SEM. A replicated surface is imaged by a four-component system, as is explained below. Different system MTFs can be determined for original and replicated surfaces. Analysis of the different system MTFs provides an optimal strategy for authentication.

The MTF is presented as a curve that quantifies the imaging accuracy of any imaging system or component as a function of spatial frequency in the scene being imaged. For most systems, the MTF curve illustrates the common-sense notion that large spatial frequencies are imaged more accurately than small frequencies. The MTF [4] is also known by the following names: contrast transfer function, sine-wave response, and frequency response.

An understanding of imaging-system accuracy as it relates to the spatial frequencies being imaged is crucial for any authentication method relying upon image comparison. For instance, if the plastic casting made a totally inaccurate impression of the original tag surface it would be impossible to authenticate this surface by comparing casting images. A surface image captured by a totally inaccurate plastic casting would not correlate well enough to discriminate the original surface imaged in the baseline examination from the image obtained in a subsequent field examination of the same surface. On the other hand, if the plastic casting made perfectly accurate copies of an original surface, it could be used to make perfectly accurate replicas of the surface. The surface topography captured by a perfectly accurate casting could be used to form a perfectly accurate replica of the original surface. Subsequent castings made from either an original tag surface or a replica surface would correlate perfectly, so the original surface could not be uniquely identified. Indeed, spatial frequency ranges that approximate totally inaccurate castings or perfectly accurate castings can be defined. Of course these spatial frequency ranges do not lead to a viable authentication, and these ranges are not used to define this method.

The MTF is used to optimize the intrinsic-surface plastic-casting method to ensure its uniqueness. Specifically, the MTF defines a spatial-frequency range

where the castings are accurate enough to authenticate an original (genuine) surface, but not accurate enough to make undetectable replicas of the original surface. It should also be emphasized that the MTF by itself does not provide a numerical image comparison necessary for authentication. The LCC and the local-sum mean must still be used to provide a numerical comparison. However, the MTF analysis leads to comparisons that provide the greatest numerical discrimination between castings made from an original surface and castings made from replicas of the original surface.

b. MTF Description

i. MTF Example

MTF curves are routinely determined and provided by the manufacturers of imaging-system components. For example, Fig. 17 presents the MTF of a particular type of photographic film (Kodak 2476). The abscissa reflects the range of discrete spatial frequencies of a special MTF test object being imaged. Each discrete frequency occupies a different region of the object scene. Furthermore, each frequency is established by a uni-directional, sinusoidally modulated gray-scale. Modulation transfer (MT) expressed in percent is the ordinate. The MT can be thought of as a numerical indication of how well the film reproduces a particular frequency from the test object. Examination of Fig. 17 shows that below a spatial frequency of ten cycles/mm the film image provides perfectly accurate object resolution. For frequencies near forty cycles/mm the film has a MT near 50%. This means that the film is midway between perfect accuracy and total inaccuracy for forty cycles/mm. At very high frequencies the MT approaches zero. So, for very high frequencies, the MT value indicates the film approaches total inaccuracy. The physical reason for this inaccuracy is that the film can not resolve features much smaller than its grain size. All imaging components have a zero MT for appropriately high frequencies. For instance, even a theoretically perfect optical lens has a diffraction-limited spatial resolution.

ii. MTF Definition

This subsection presents a simplified definition of the MTF. The MTF curve describes the dependence of the MT upon spatial frequency. At each frequency, the MT defines how the object sinusoidal gray-level is transferred to the image.

Each of the object gray-level variations in the x spatial coordinate has a sine dependence upon spatial frequency (f) according to:

$$G_o = O_1 + O_2 \sin(2\pi f x) \tag{4}$$

O_1 and O_2 are the constant and amplitude of the gray-level sine variation, respectively. The object modulation at spatial frequency f is defined as:

$$M_o(f) = O_2/O_1 \tag{5}$$

Each image gray-level spatial variation is:

$$G_i = I_1 + I_2 \sin(2\pi f x) \tag{6}$$

I_1 and I_2 are the constant and modulus of the image gray-level sine variation, respectively. The image modulation M at spatial frequency f is:

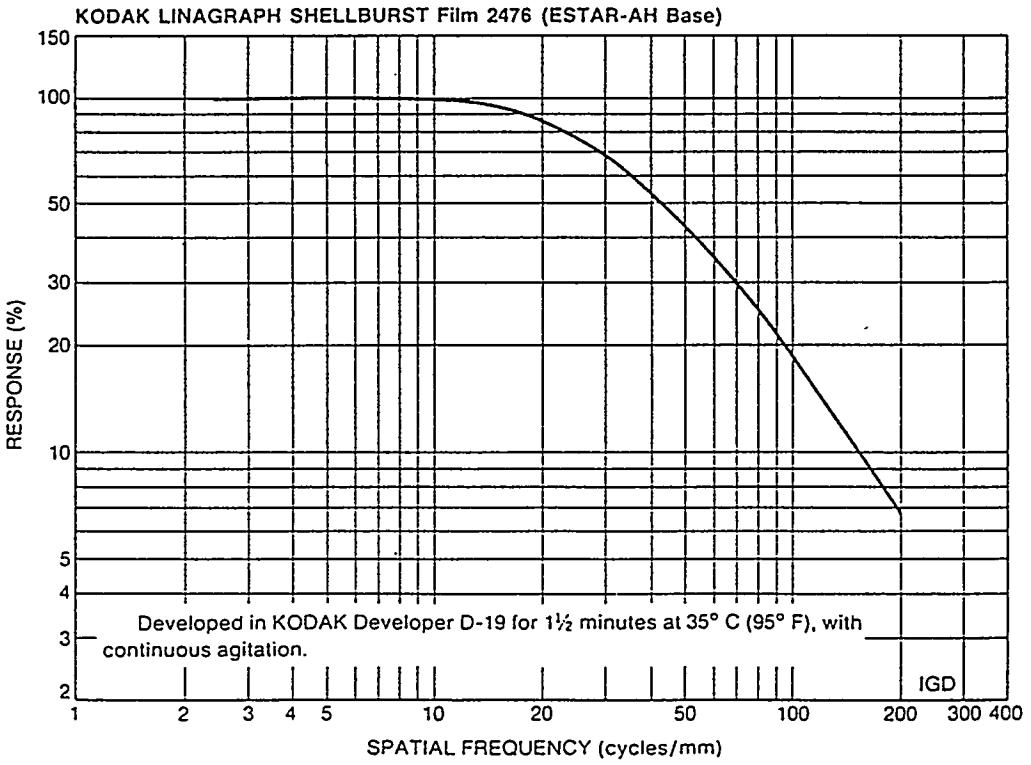

Fig. 17. Example of a MTF Curve for a Photographic Film

$$M_i(f) = I_2/I_1 \quad (7)$$

The modulation transfer, MT, at spatial frequency f is:

$$MT(f) = M_i(f)/M_o(f) \quad (8)$$

The modulation transfer function, MTF, is the frequency dependence of the MT.

iii. MTF System Product Rule

The MT of an imaging system at each frequency is the product of the MTs of its individual components at that frequency. The modulation transfer of a n-component imaging system, MT_{sys}, is:

$$MT_{sys} = \prod_{c=1}^{n} MT_c \quad (9)$$

For example, a camera is an optical system whose individual components are a film and lens. Therefore, at each frequency, the MT of the camera is the product of the film MT times the MT of the lens, as graphically illustrated in Fig. 18. The camera MTF is then the function defining the frequency dependence of the system MT.

c. MTF-Optimized Authentication

For either the baseline or the field inspection, the components of the imaging system used to image an original surface consist of a single plastic casting and an SEM. According to Eq. (9), the modulation transfer of the original (genuine) system, $MT_{or,sys}$ is:

$$MT_{or,sys} = MT_{ca}MT_{sem} \quad (10)$$

MT_{ca} is the casting modulation transfer, and MT_{sem} is the SEM modulation transfer. Since $MT_{or,sys}$ is determined for each spatial frequency, the modulation transfer function of the original system, $MTF_{or,sys}$, can be formed for all frequencies. Figure 19 graphically shows $MTF_{or,sys}$ as a product of the system component MTFs. This figure illustrates that the $MTF_{or,sys}$ is determined as a first-generation image of the original surface.

For a field inspection on a replicated surface, the components of the imaging system consist of a replicated negative made from the original surface, a replicated tag positive, an authentication casting, and an SEM. According to the product rule, the modulation transfer of the replicated system, $MT_{rp,sys}$, is then:

$$MT_{rp,sys} = MT_{neg}MT_{pos}MT_{ca}MT_{sem} \quad (11)$$

MT_{neg} and MT_{pos} are the modulation transfers of the negative made from the original and the replicated positive, respectively. Figure 20 graphically shows $MTF_{rp,sys}$ as a product of its system component MTFs. This figure illustrates that the $MTF_{rp,sys}$ is determined from a third-generation image of the original surface.

Figure 21 plots the original system and the replicated system MTFs from Figs. 19 and 20, respectively. It should be emphasized that these MTFs were not directly determined, but were approximated from the results of the replication experiments

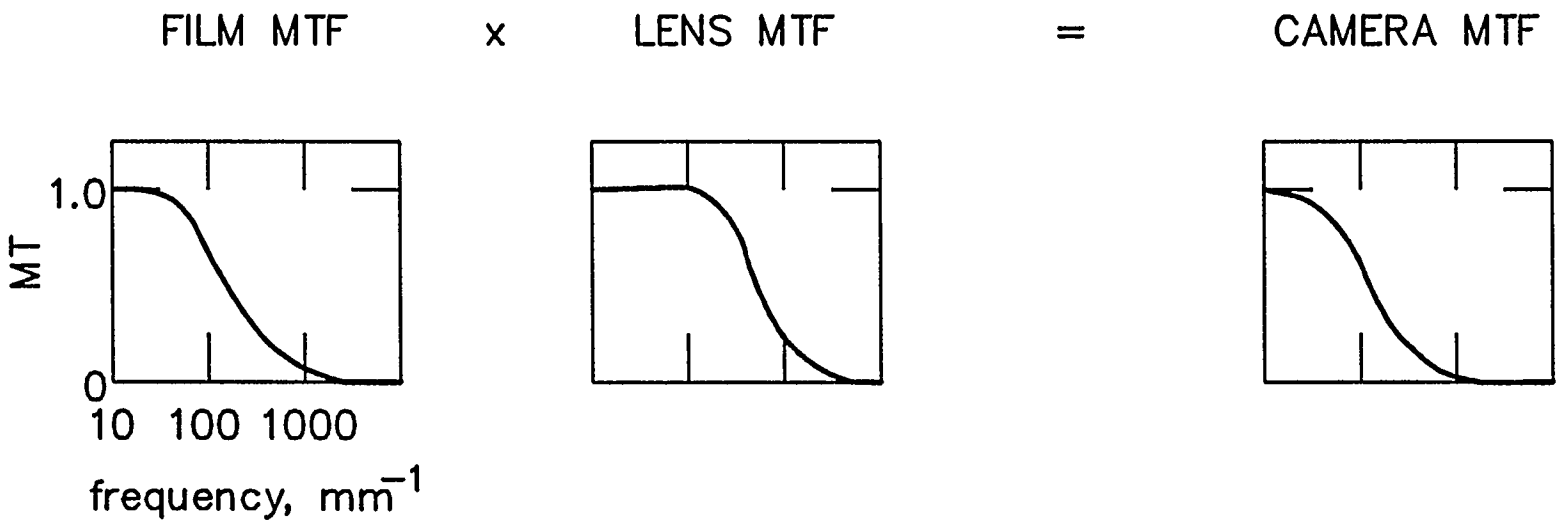

Fig. 18. MTF System Product Rule Illustrated for a Camera

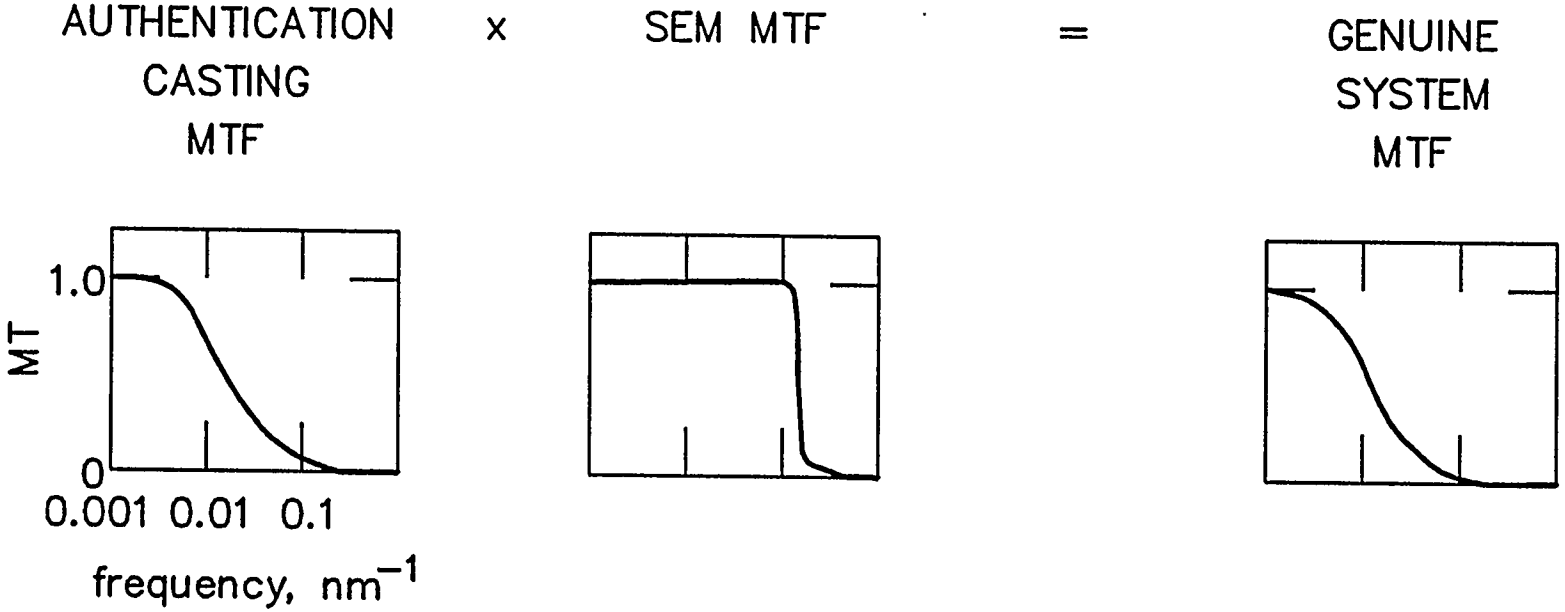

Fig. 19. Original (Genuine) Tag MTF

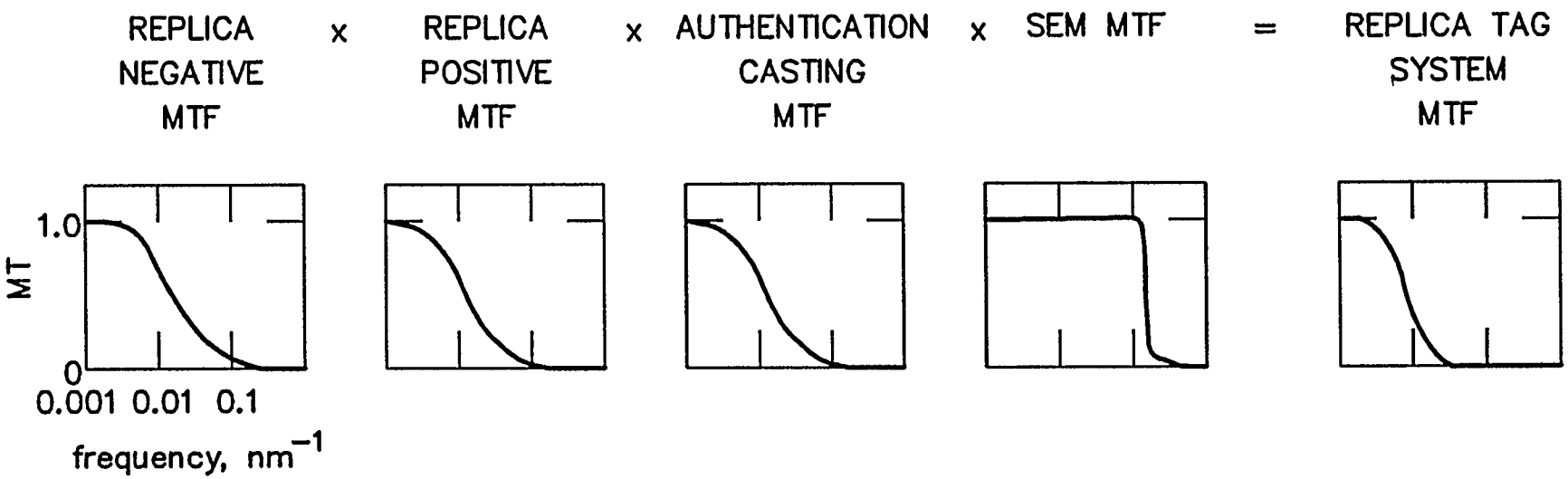

Fig. 20. Replicated Tag MTF

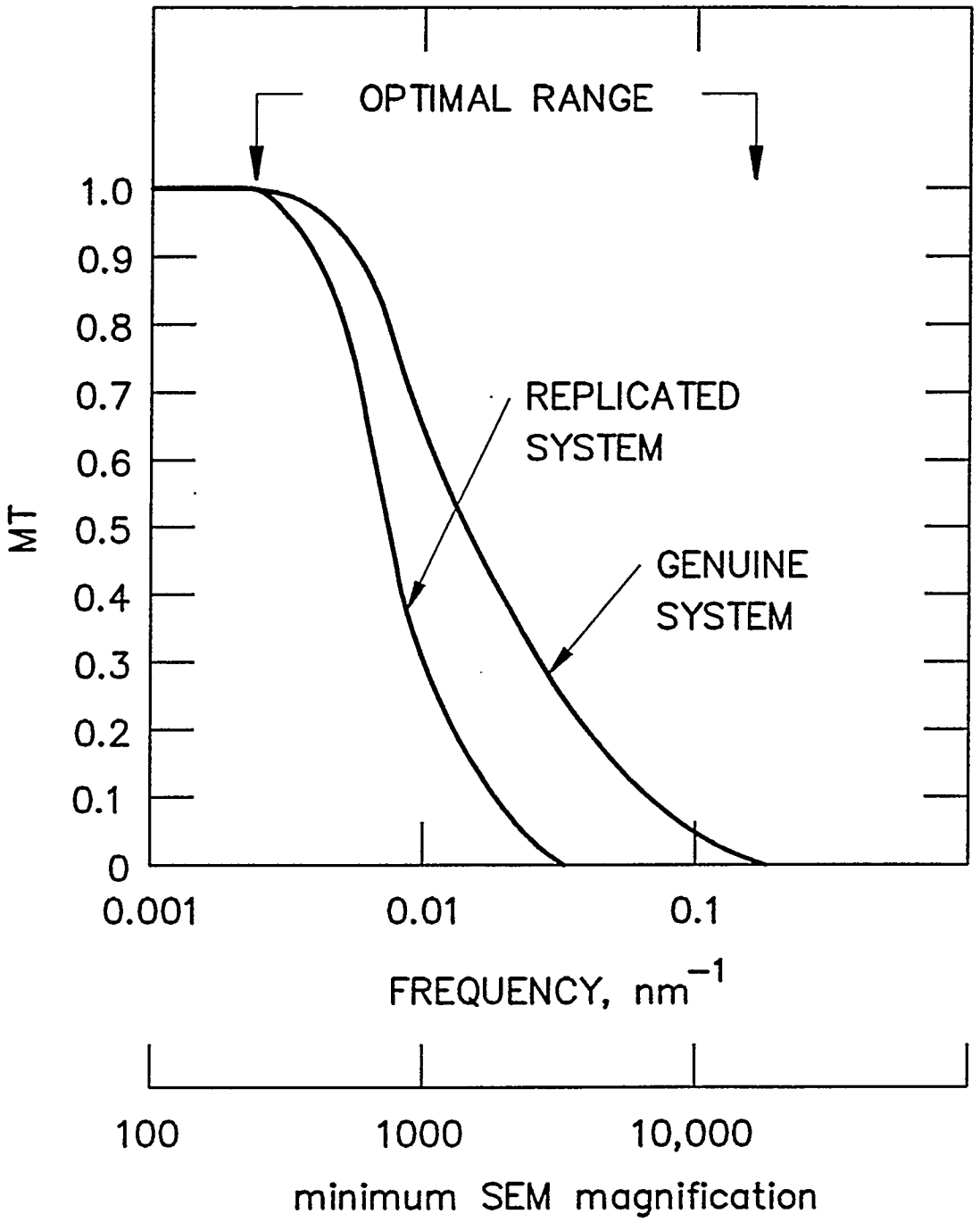

Fig. 21. MTF Optimized Tag Surface-Topography Frequency and Examination Magnification

presented in Section II.D. Figure 21 indicates that the optimal spatial frequency range for authentication corresponds to the range $1>MT_{or,sys}>0$. In this range, $MT_{or,sys}>MT_{rp,sys}$, and the frequency is not beyond the resolving power of the genuine system. Figure 21 graphically expresses that a third-generation plastic casting made from a replicated surface results in a lower system MT than the first-generation casting made from a genuine surface. Replication errors compound with each generation, and this is expressed by the inequality $MT_{or,sys}>MT_{rp,sys}$ in the optimal frequency range. The abscissa in Fig. 21 also shows a minimum SEM magnification that can resolve the spatial frequency. This brings in the need to operate the microscope near a magnification that resolves differences between original and genuine surfaces.

Some simplifying approximations are now made to extend this analysis. If the negative made from the original, the replicated positive, and the plastic casting are assumed to have the same modulation transfer, then:

$$MT_{neg} = MT_{pos} = MT_{ca} \tag{12}$$

The justification for $MT_{neg} = MT_{ca}$ is that they both must be formed in the liquid state from a plastic material. A plastic is necessary, because the negative and the casting must be deformable enough to be separated from a microscopically rough surface in one piece. Although a more accurate positive can be formed from the vapor state, the replicated positive could also be formed from the liquid state. If it is formed from the liquid state, the approximation, $MT_{pos} = MT_{ca}$, can be made.

Another approximation is to set the modulation transfer of the SEM to one in the range $1>MT_{ca}>0$.

$$MT_{sem} = 1 \tag{13}$$

The validity of this assumption depends upon the resolution of SEM used to image the casting. It is likely to be valid for a high-resolution field-emission SEM.

Combining Eqs. (12) and (13) with Eqs. (10) and (11) results in the following approximations to the system MTFs:

$$MT_{or,sys} = MT_{ca} \tag{14}$$

$$MT_{rp,sys} = MT_{ca}^3 \tag{15}$$

Optimization of the imaging conditions can be quantified by determining the maximum difference between $MT_{or,sys}$ and $MT_{rp,sys}$ as:

$$\frac{d}{dMT_{ca}} (MT_{or,sys} - MT_{rp,sys}) = 0 = 1 - 3MT_{ca}^2 \tag{16}$$

The maximum difference occurs for a spatial frequency with a $MT_{ca} = 0.577$. Indeed, the range of spatial frequencies around this frequency also provide useful discrimination of genuine from replicate surfaces. The most significant differences between castings made from an original and castings made from a replica occur for spatial frequencies in this range. Therefore, authentication is optimized for a range of spatial frequencies that correspond to MTs near 0.577.

Since the MTF analysis determined a range of optimal spatial frequencies, it is now possible to state three particulars that provide the most favorable authentication.

* Select the surface marking device to maximize the density of the optimal spatial frequencies. For example, the grit size of the sandpaper used to form the original surface topography should be selected to maximize features in the optimal spatial-frequency range.

* Select an SEM magnification that resolves the entire optimal spatial-frequency range.

* Compare the digital baseline and field-inspection images, with weighted spatial frequency. Zero weight would be given to spatial frequencies for $MT_{or,sys} = 1$ or $MT_{or,sys} = 0$. Maximum weight would be given to the frequency corresponding to the maximum difference in $MT_{or,sys} - MT_{rp,sys}$. This maximum weighted spatial frequency has an $MT_{ca} = 0.577$ under the approximations discussed in the derivation of this frequency. The linear correlation coefficient obtained from a frequency-weighted image would have better discrimination than the unweighted LCC. It may be possible to discriminate genuine from replicate images solely from the weighted LCC. Implementation of the spatial weighting is relatively straightforward, since the unweighted LCC is already determined from frequency (Fourier) space. A weighted LCC could easily be calculated from the Fourier transforms of the registered images.

2. Use of the MTF to Interpret Replication Experiments

a. SEM Magnification

At lower SEM magnifications, the MTF analysis predicts that it would not be possible to discriminate original from genuine surfaces. This is because low-magnification images do not contain enough information from the optimally discriminate spatial frequency range. Figure 22 shows a lower magnification view of an original (top) and two replicas of the same area. The SEM magnification used to obtain these images was 700X. Visual comparison of the replicas shows none of the bright ridge-line imperfections visible at higher magnifications. The local-sum statistic (see Section II.B), designed to evaluate bright features, does not discriminate between the original and the replicas at low magnification. Spatial frequencies resolved at the lower magnifications have a casting modulation transfer nearly equal to one, so the difference in modulation transfer between the original and replica is very small.

b. Replica Formation State, Surface Roughness, and MTF

When attempting to make high-quality replicate positives it is important to form both the negative and the positive replicas by means that ensure the best-possible MTF. Given a choice between liquid and vapor state replication processes, the better process would have a finite MTF at higher spatial frequencies. For reasons discussed in Section II.B, high quality negatives were formed by a liquid-state, acetone-solvent, cellulose-acetate solute system. However, microscopists agree that replicas formed from the vapor state locally reproduce a surface better than those formed from the liquid state. Use of the vapor state to form the negative replica for a few-square-centimeter surface is precluded because the surface is both rough and large from a microscopic viewpoint.

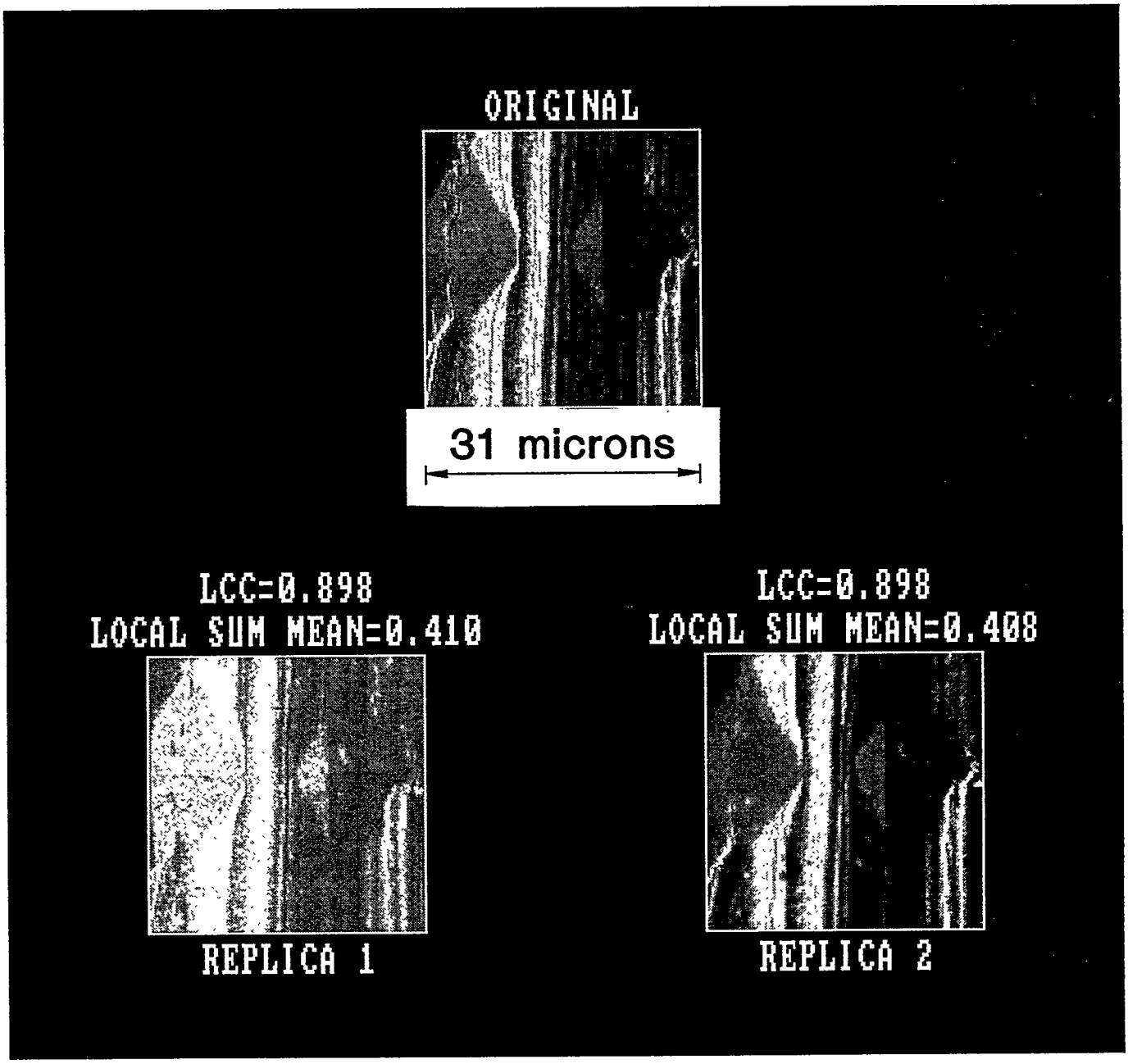

Fig. 22. Original and Two Replicas at Low Magnification

A negative replica, formed from the vapor state, would tear and deform upon separation from the original surface. However, the positive replica can be made from the vapor state (see Fig. 2), since the negative can be dissolved without deforming the positive.

Figure 23 shows SEM images of a weld and a positive weld replica made by Sandia National Laboratory [5]. This weld and the positive replica were used to assess an optically authenticated, intrinsic-weld tag proposed by Martin Marietta, Oak Ridge, Tennessee. The SEM images were supplied to ANL for a preliminary evaluation of surface replication. Both the positive in Fig. 23 and its associated negative replica are formed from the liquid state. Examination of Fig. 23 shows the replica features are consistently broader than the original weld. This broadening produces a dark border around all the features in the subtraction image (original minus replica) at the right side of Fig. 23.

Even though the magnifications in Figs. 22 and 23 are comparable, there is little evidence of feature broadening in Fig. 22. Both negative replicas used to produce Figs. 22 and 23 were formed from the liquid state. However, the Fig. 22 positive replica was formed from the vapor state, while the positive in Fig. 23 was formed from the liquid state. The conclusion drawn from comparing Figs. 22 and 23 is that the vapor state exhibits a better MTF than the liquid state.

c. Summary of MTF Analysis

The modulation transfer function, a first principle imaging concept, was used to analyze experimental surface-replication results. This function revealed how the surface uniqueness is optimized for a specific spatial-frequency range. Both the surface topography and authentication magnification must be chosen to emphasize features in the optimal range. In addition, a linear correlation coefficient, weighted to emphasize only optimal-range surface features, could provide increased discrimination between original surface castings and castings made from counterfeit surfaces. The MTF is a valuable concept for the successful authentication of the intrinsic-surface, plastic-casting method.

B. External Analyses

1. General Comments on LANL Effort

a. History of LANL Effort

Los Alamos National Laboratory (LANL) was charged with adversary analysis of the plastic-casting, intrinsic-surface tag. Specifically, the tag was analyzed for use in START. LANL began the work in late 1990.

By mid-1991 LANL had prepared pairs of original and positive-replica surfaces. These surface pairs were never presented to ANL for a casting authentication exercise. By April 1993 a second set of original and positive-replica surfaces were prepared. The second set of surface pairs was also not presented to ANL for a casting authentication exercise. Rather, in April 1993, LANL sent castings made from the second set of surfaces to ANL. ANL began but did not complete examination of these castings.

LANL developed its own image-alignment software by mid-1991. A rigorous comparison of both LANL and ANL software packages was completed in June 1991. LANL

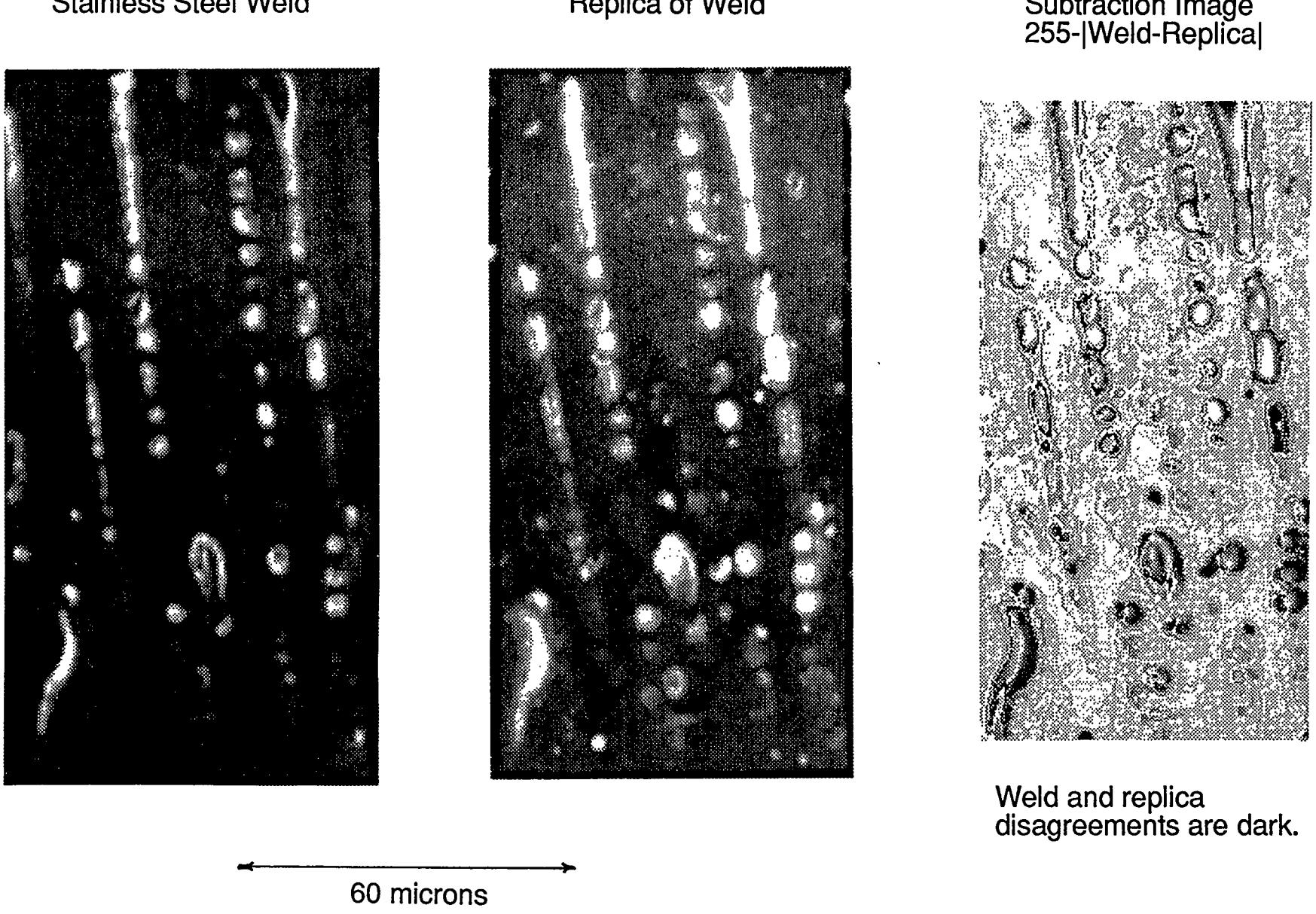

Fig. 23. SNL Replication of a Weld

revised its software, and submitted new images to ANL in April 1993. Results of both these software comparisons are discussed below.

b. Improved Adversary-Analysis Procedure

For treaty verification, tagging would be used to authenticate a TLI by comparing the baseline signature with subsequent field-inspection signatures. For most treaty scenarios the inspecting side gathers the signature from both the baseline and field inspections. In addition the TLI presented to the inspecting side in the baseline inspection is defined as the true TLI. Therefore, when a tag is authenticated the inspecting side knows which is the baseline signature and which is the field-inspection signature. For the purpose of a generic-treaty authentication exercise ANL is demonstrating a surface-authenticated tag. LANL is the owner of the original and replicate tag surfaces. Therefore, ANL is the inspecting side and LANL is the inspected side.

The procedure LANL used to conduct the adversary analysis conflicts with the generic-treaty implementation of a tag. For the 1993 adversary exercise LANL, as the inspected side, gathered the inspection signatures which are the castings. As the inspecting side ANL should be gathering the inspection signatures. Furthermore, since one casting in each pair submitted to ANL was not identified as the baseline casting, the inspected side (LANL) did not even identify the baseline casting. This also violates a generic treaty tagging scenario. ANL, as the inspecting side, would always know which was the baseline casting.

ANL continues to propose an authentication exercise based upon a generic-treaty tagging scenario. LANL should present unmarked original surfaces to ANL. ANL, as the inspecting side, would mark the surfaces and make the baseline castings. Then, ANL would return the original surfaces to LANL. LANL would fabricate the positive replica surfaces. Then ANL, as the inspecting side, would make castings from pairs of surfaces presented to it by LANL. These surfaces could be either the original or replicate surfaces. Castings made from these surface pairs would be the field-inspection castings. ANL would then authenticate the surfaces by comparing the field inspection and baseline castings.

At this point ANL would agree to a preliminary authentication exercise based on LANL presenting the surfaces it has already fabricated to ANL. LANL would first present the original surface, and ANL would make the baseline casting. Then LANL would present additional surfaces that could be either the original surface or a positive replica. ANL would make the field inspection castings from these additional surfaces. Then, ANL would authenticate the surfaces by comparing the field inspection and baseline castings.

c. Image-Alignment Software Comparisons

Baseline and field-inspection SEM image data sets must be aligned before authenticity can be determined. Translation, rotation and magnification alignments must be addressed. The best alignment is determined by the highest correlation. Alignment is accomplished by systematically searching though translation, rotation, and magnification differences between two data sets. The necessity for alignment arises because the baseline and field inspection castings can not be positioned in exactly the same position with respect to the SEM electron beam.

ANL and LANL use different alignment software. ANL uses Semper and LANL uses PV WAVE. Both software packages provide a variety of high level commands. ANL and LANL combine these commands to produce an alignment program.

ANL has interacted twice with LANL concerning alignment software. The first interaction ended in June 1991. LANL submitted several image data set pairs to ANL. These image pairs were of a similar scene which means that they were either from an original or a replicate. There were translation, rotation, and magnification differences between each pair. Each pair was a 512 by 512 pixel image, and the software was compared by aligning five 128 by 128 sub-images from a typical pair. The results of the first interaction are listed in Table 2.

Table 2. Correlation Comparison for ANL and LANL Software

Linear Correlation Coefficient			
Correlation Pair	ANL	LANL	Percent ANL > LANL
1	0.807	0.696	15.9
2	0.891	0.792	12.5
3	0.845	0.822	2.8
4	0.891	0.797	11.8
5	0.917	0.888	3.3

Alignment correlations from ANL software averaged 9.3% higher than LANL software. ANL concluded that its software is doing a better search for alignment, and this resulted in higher correlations. However, two of the correlations were only ~3% higher while the other three were 12 to 16% higher. So there was also a wide variance in the search quality of LANL software.

A second software comparison was initiated by LANL in April 1993. Twenty-five pairs of 512 by 512 pixel images were submitted to ANL. ANL determined that 22 pairs were pixel by pixel identical as if one image was created from the other using a computer copy command. None of these twenty-five pairs were suitable for an alignment software comparison since they were not of similar scenes with shift, rotation and magnification differences.

Another aspect of software comparison must be emphasized. Both software packages align specific 128 by 128 pixel sub-regions from two 512 by 512 pixel input images. One of these 512 by 512 images represents the baseline and the other represents the field inspection. The first 128 by 128 image is merely copied from some user-selected sub-region of the larger baseline image. The second 128 by 128 pixel image is extracted from the larger field-inspection image based upon the alignment software search. A valid software comparison must use the same baseline sub-region; careful attention to this imperative was adhered to in the June 1991 software comparison. For the April 1993 images LANL did not supply a list of coordinates from one image in each pair necessary to assure that the same baseline sub-region could be compared.

LANL has not demonstrated that its correlation software is better or even as good as ANL software. On the contrary, Table 2 implies that LANL software does not optimally search for the best shift, rotation, and magnification alignment. No useful software comparison can be attained from the April 1993 data set pairs because they did not have any alignment differences.

Any conclusions that LANL draws from its correlations are questionable since its software does not search well enough to find the peak-correlation. Thus, two surfaces that it evaluates may actually correlate better than LANL reports. Moreover, the variance in correlation between several pairs of surfaces is less than LANL reports because the quality of its search is randomly better or worse for different data set pairs.

ANL proposes a rigorous test of both alignment software. Both sides should submit image data pairs to each other. ANL has some original-replicate pairs that were difficult to search for peak correlation. Undoubtedly, LANL also has some interesting pairs. There must be shift, rotation, and magnification alignment differences in most of the data set pairs to be evaluated. Designation of one image in each pair as the baseline should be made. For each baseline image the central x,y coordinates of each 128 by 128 sub-region to be compared must also be supplied. A third correlation software package should be introduced if an appropriate one can be identified. The third software package could be used as confirmation to ANL and LANL software.

d. Full Replication

Full replication requires that an inspector cannot distinguish the positive-replica material from the original TLI surface. Specifically, the positive replica must appear to have the same reflectance and color as the original TLI surface. At this time LANL has prepared aluminum-alloy original surfaces and epoxy positive-replica surfaces. LANL must prepare metallic positive-replicas to complete the replication. Moreover, LANL must also demonstrate that a metallic positive-replica can be seamlessly blended into a larger aluminum-alloy surface. Full replication is necessary to complete the adversary analyses.

2. ANL Response to LANL Reports

a. LANL Reports

LANL has written three reports. The first report [6] was classified and covers early LANL work in 1990 and 1991. ANL wrote a classified response [7] to this report in February 1992. A second classified report [8] covers LANL work in 1992 and 1993. An unclassified report [9] based on the later work was also issued by LANL.

b. Selected Findings of Latest LANL Unclassified Report and ANL Response

Selected quotes of findings from the LANL unclassified report [9] are italicized below. The ANL response to each finding follows in non-italicized text.

i. Surface Changes

> *The object did change during the experiment. The images shown in Fig. 1 were taken at a magnification of 1000x and were centered on the area examined at higher magnification. Note that the features*

labeled A and B in the first image are missing from the second image. Feature A may have been an individual grain of aluminum that was dislodged during replication or cleaning. Feature B was a feathery structure that was formed during making of the surface. Part of that structure disappeared. The most probable cause of these changes was removal of small pieces of the object during replication. Such changes could occur during cleaning and handling, and as will be discussed later, they could come from reaction with the environment. [9, p. 5]

On close examination of the matrix of correlation data, the value of the correlation between image pairs appears to decrease with increased number of replications. [9, p. 11]

The fit of the data is shown in Fig. 2. The error bars are the standard deviations of the averages of the diagonal matrix values. Although the noise level is high, there is a statistical degradation in our ability to make replicas from a single object surface. The value of "C" in Eq. 2 implies that a limiting LCC of 74% would be reached after many replications. [9, p. 13]

Although some damage continues to occur during repeated replications, most of the damaged areas were intentionally avoided by the SEM operator. The direct observation of the surface of the object does not show significant change in the recorded areas during these experiments. The drop in LCC as a function of the number of replications therefore seems to be related to our ability to replicate rather than to changes in the original surface. It is not unreasonable to expect this type of effect to occur. The fidelity of the replica depends first on the ability of the softened cellulose acetate to wet the surface and second, on the ease with which the cured acetate can be removed from the surface. Both of these subjects are related to the cleanliness of the surface being copied. Changes in the molecular film of contaminants on the surface of the object can indeed affect the wetability and ease of removal. At the same time, if the contaminant film is only a few molecules thick, then the primary and secondary electron flows will not be greatly affected, and the image will appear to be unchanged. [9, p. 13]

LANL findings show two effects of the cellulose-acetate castings interacting with the original tag surface. The first effect, described by the photomicrograph in their Fig. 1, relates to micro-debris associated with the sandpaper marking of the tag surface. A second effect, described by the graph in their Fig. 2, is associated with the method LANL uses to make cellulose-acetate castings.

The first effect is dealt with by discarding the first casting after the tag is initially formed on a tag surface. LANL is referring to the tag surface when discussing changes in the object. In addition, LANL uses replica for casting in their description. Initial surface marking with sandpaper results in large amounts of loosely-adherent tag debris. This debris is composed of sandpaper grit as well as tag material. Large features removed by the first casting made by LANL, as shown in their Fig. 1, are examples of debris. ANL authentication procedure does not use the first casting. This casting is discarded as described in Section II.E.1.a of this report.

The second effect is described as an insignificant change in the surface. This change is subtle and not due to large missing features. The second effect is largest between the first and second casting and has largely dampened out by the fifth or sixth casting as evidenced by their Fig. 2.

In order to further discuss the second effect it is necessary to describe the different methods ANL and LANL use to make castings. ANL uses the "dip" method as described in Section II.E.1.c. The dip method requires that the cellulose acetate tape be dipped in a beaker of acetone, held in the acetone until the tape softens, and then laid out over the surface. LANL uses the "drop" method. The drop method involves placing drop(s) of acetone on the surface to be cast, and then pressing the cellulose acetate tape into the surface. Once again, LANL is not following the ANL authentication procedure.

ANL interprets LANL results reported in their Fig. 2 as due to micro-yielding of the fine surface scratches associated with pressing the acetate into the surface. This pressing causes the fine scratches to yield and move slightly during the first few castings. The yielding is largest for the first casting because the surface yield strength is lowest. This is why the effect is most noticeable between the first and second castings. The first few castings cold-work the surface and raise its yield strength. Eventually the yield strength is raised enough, so the surface material can withstand the pressing associated with making additional drop method castings. Therefore, after a few castings there is little surface change, and by the sixth casting this effect is minimal.

ANL does not notice these subtle changes because the dip method relies on surface tension to draw the acetate into the fine scratches. In addition, ANL has investigated making castings by both the dip method and drop methods. ANL results indicate that the dip method provided better resolution of the fine surface scratches. The better results of the dip method are attributed to a more uniform, micron-scale, solvent-solute distribution over the tape surface at application. Microscopists, having extensive replication expertise, prefer the dip method because it reproduces finer surface details. The dip method is also operationally superior, since it is possible to cast vertical surfaces. Because the acetone would run off before the tape can be applied, the drop method can not be used on vertical surfaces.

ii. Stress Corrosion

> *The marking process imparts potential energy to the surface that is manifested by an increased chemical reactivity. Should the surface later be exposed to reactive chemical species, the chemical reactions will be concentrated on the sharp edges and boundaries on the surface that are the prime features in an image. These microscopic structures on the surface are most open to attack by stress corrosion.* [9, p. 16]

ANL does not recommend tagging highly-stressed surfaces used in corrosive environments if the surface material is sensitive to stress corrosion.

iii. Surface Protection

> *The test objects for this study were prepared from 6061 aluminum alloy. The surface of the objects was roughened by light sanding with 150-grit sand paper, then a fiducial pattern was scratched on*

the surface with a scribe. After the objects were examined in the SEM, they were attached to the exterior of Building TSL 30 in Technical Area 46 at LANL. One object was attached to the north face of the building and the other to the south face of the building. Both objects were in partially shielded locations and protected from wind-driven sand and precipitation by plastic bags; otherwise the objects were exposed to the atmosphere. [9, p. 17]

As discussed in Section II.E.1.a, ANL covers the surface with an adhesive label (there is no adhesive directly over the tagged surface). The label greatly reduces the amount of corrosive gases that contact the surface compared to the plastic bag used by LANL. Since LANL did not protect the surface adequately, their corrosion results are not relevant.

iv. SEM and Optical Image

However the brightness of an "image" does not bear a simple relationship to the brightness seen in an optical image. [9, p. 21]

The word image in quotes above refers to an SEM image. At low magnification and for objects with a minimal depth-of-field, SEM and optical images can be directly compared [10, p. 5]. The result is that both images are very similar if the optical image is illuminated in a certain way. Specifics of this illumination are discussed in Section II.C.

v. Replica Material and Modulation Transfer Function

Palm and DeVolpi also assume that the negative made from the original object (original replica), the replicated tag positive (copy), and the replica of the positive copy (copy replica), have the same MTF. This assumption is not correct. No MTF is associated with the objects being examined by the SEM. The concept of an MTF only applies to an imaging system. [9, p. 22]

LANL is referring to use of the modulation transfer function (MTF) to optimize tag authentication. MTF arguments were reported previously [1] by ANL. Section VI.A.1.c presents the same arguments.

ANL asserts that replication materials have an MTF. The MTF is a broad concept applicable to any imaging instrument or media no matter how it forms an image. As discussed in Section VI.A.b.i, it is routinely used to determine the resolution of photographic film types. A film MTF can be determined from the image formed by contact printing [11] an MTF test-object on the film. The film MTF test-object has several, two-dimensional, discrete-frequency, sinusoidally-varying, gray-scale features. High object frequencies are generally reproduced on the film image less accurately than low frequencies. Different MTFs are determined for each type of photographic film.

Each replication material is no less an imaging system than each type of photographic film. The analogy between making a replica and contact-printing photographic film is obvious. In principle a replication test-object with several, three-dimensional, discrete-frequency, sinusoidally-varying features could be prepared. This object would be analogous to the film MTF test-object. Replicas made from the replication MTF test-object would contain three-dimensional images of each object frequency. High frequencies would be replicated less accurately

than low frequencies. Different MTFs would be determined for each type of replication material.

vi. Histogram Equalization

> *Once it was realized that histogram equalization of the image data offered no advantage the practice was discontinued because it added to the computation times.* [9, p. 32]

> *orig = hist_equal(aa(0)); histogram equalize the image*
> *copy = hist_equal(bb(0)); histogram equalize the copy image*
> [9, p. 33]

The first quote is not quite an accurate statement. There is a definite disadvantage to histogram equalization. ANL and early work by LANL [12] determined that histogram equalization resulted in significantly lower correlations. The LANL work was communicated to ANL; it showed correlations were lowered by an average of 15% if histogram equalization was used compared to no equalization. ANL understood that histogram equalization was removed from the PV WAVE coding used for the ANL-LANL software comparison reported in Table 2.

The second quote indicates that histogram equalization has reappeared in the latest PV WAVE coding. An ANL staff member [13] familiar with PV WAVE has reviewed the entire source-code. The conclusion is that LANL is histogram equalizing both the baseline and field-inspection images ("orig" and "copy") before calculating a correlation.

VII. RECOMMENDATIONS FOR FURTHER DEVELOPMENT

A. Introduction

The previously-described surface-inspection techniques, casting-examination hardware, and image-comparison software are sufficient to provide proof-of-principle authentication for the intrinsic-surface plastic-casting method. Additional work should be performed in several areas to advance this method. These areas are: assembly of a high-throughput casting authentication system; improved authentication algorithms; improved adversary analysis and application-specific environmental testing. These items are described below.

B. High-Throughput Casting Authentication System

1. Amount of Data Needed to Authenticate

In order to discuss the throughput of an image-based authentication method, it is important to establish the amount of data needed to authenticate a surface. However, the amount of data has not been established for this authentication method. Section II.B.5 mentions the need for an overall pass/fail criteria based on the percentage of subareas that meet both correlation and local sum criteria. This criteria would define the necessary number of authentication subareas. The number of subareas and the size of each also define the necessary amount of data. Determination of the necessary data awaits an authentication exercise that compares castings made from original and positive-replica surfaces. For the purpose of defining a high-throughput authentication system here, it is assumed that nine high-magnification 512 by 512 pixel images would be needed. These nine images would result in 144 authentication subareas, 128 by 128 pixel square.

2. Limitations of Proof-of-Principle System

The existing proof-of-principle system has a throughput too low to support a large authentication regime. Although the operator can easily choose a topographically appropriate subarea on the baseline casting, it is time-consuming to locate the corresponding subarea on subsequent field-inspection castings. It should be appreciated that at 5,000X, only 0.00054% of the tag surface is visible in the 512 by 512 pixel digital-image display. Moreover, the casting topography appears monotonous to a SEM operator, so any given subarea does not immediately appear to be distinctive.

With some effort, each corresponding baseline-casting subarea is located on the field-inspection casting by zooming in on the field-inspection casting subarea using a series of ascending magnification baseline images. Each baseline authentication image is acquired at 5,000X. Before moving the microscope stage, a series of lower magnification images (lowest is 35X) is acquired. Clear-plastic baseline overlays (from viewgraph stock) are prepared from the lower magnification images.

When a field-inspection casting is examined in the SEM, the lowest magnification baseline overlay is placed on the CRT of the SEM, and the lowest microscope magnification is selected. The operator can then visually align images to relocate the corresponding high-magnification authentication subarea in a three-step process. First, the operator adjusts the CRT brightness, so both the baseline overlay and the field-inspection CRT images are visible. Then, the operator moves the SEM stage to align common image features. Finally, both SEM and overlay

magnifications are increased until the authentication magnification is reached; minor stage adjustments are necessary at each increasing magnification.

Throughput is low because the operator performs a tedious sequence of manipulations with the microscope stage and magnification controls. Other limitations of the proof-of-principle system are slow image-correlation hardware and the limited storage available for digital images. It is estimated that two field-inspection castings per week could be authenticated with the existing equipment. This estimate is based upon an eight-hour day and two full-time workers.

3. Description of High-Throughput System

Both the features and operation of a highly automated SEM, image processor, and image-storage system are described. This advanced system would provide casting-sample throughput suitable for the examination of thirty castings per week, based on an eight-hour day for a full-time worker. Further increases in throughput would be met by duplicating the system. Figure 24 is a schematic describing each advanced system.

Features included in each advanced-system are:

* Automated control of the entire authentication process from a central computer executing one computer program. The central computer would control SEM stage movement, other SEM functions, and interface with archival image storage. This computer also performs image correlation and provides the quantitative authentication.

* Automated SEM stage movement is included. The SEM stage is moved by motors controlled by a dedicated stage-automation computer. This stage computer accepts commands from and provides stage movement information to the central computer via a serial line.

* Control of all the SEM functions (e.g., change of magnification, brightness, contrast, digital image acquisition by the SEM framestore, etc.) by a computer-controlled SEM that accepts external control commands. The SEM computer communicates via a serial line with the central computer that provides control commands. Furthermore, a recently acquired digital image residing in the SEM framestore is transferred to the central computer via a parallel line to an interface card in the central computer. This interface-card image is recognized by the central computer as a virtual disk, and is then accessible by the central computer's main program.

* High-capacity optical storage for archived baseline casting images is provided. These archived images are recalled for correlation with recently acquired field-inspection casting images.

All the components of the advanced system are commercially available products. The components would be integrated into a system by ANL.

An operational description of the advanced system is described. For the baseline casting, the SEM operator would pick out the topographically appropriate baseline casting subareas; although this feature might also be automated. The operator can move the stage with a joystick control supplied with the motorized stage control system.

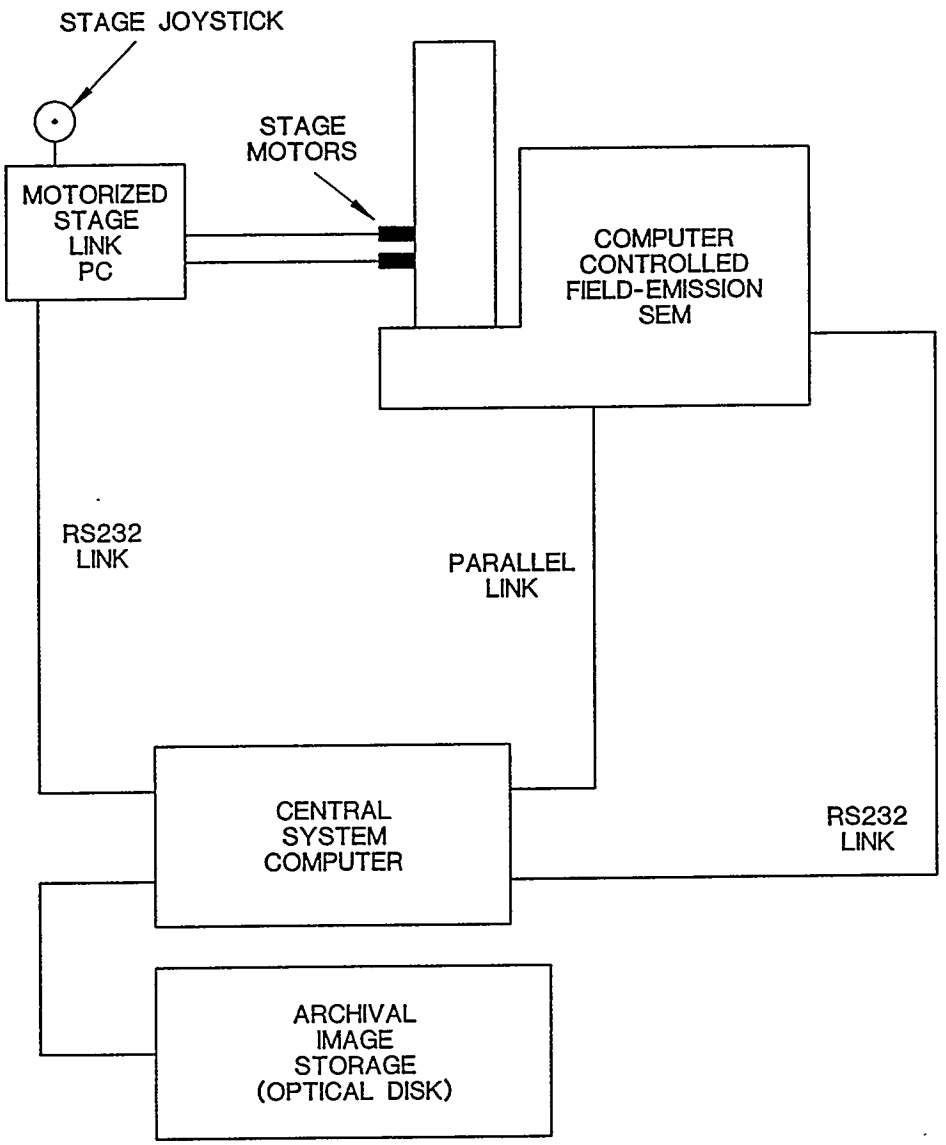

Fig. 24. Schematic of High-Throughput System

Locating each high-magnification subarea on field inspection castings is totally automated. Specifically, several low-magnification images would be saved from each baseline casting examination. These images would be used to guide the stage to the high-magnification authentication subareas by an iterative process. First, the distances the motorized stage moves between high-magnification subareas on the baseline casting would be saved. Then a low-magnification view around each subarea would be saved from the baseline examination. When the field examination casting is examined, the baseline stage movements will be used to guide the stage between successive subareas. At this time, a low-magnification view around the subarea will be acquired and correlated with the corresponding low-magnification view of the baseline examination. The shift difference determined from this correlation would be used to finely adjust the stage, so the high-magnification view of the field casting will correspond with the high-magnification view of the baseline casting. Of course, only the high-magnification views would be used for numerical authentication.

4. Specific Component Description

Commercially available components are described. Mention is made of specific brands and models only to establish commercial availability.

a. Central Control Computer and Software

A generic 80486-66 Mhz PC has adequate performance. The control program is written in the high-level Semper image-processing language described in Appendix A. A recent Semper upgrade allows for issuance of commands and reception of information from two separate serial ports. One port would communicate with the SEM, and the other port with the stage-control PC. Semper also includes the ability to incorporate user-written Fortran or C-language commands. This is useful if more efficient algorithms replace the Fourier transform based image-correlation software. The Semper program speed is upgraded by running it on a Sprynt card that resides in one of the PC expansion slots. The Sprynt card is supplied by Synoptics, Ltd. as is the Semper software. This card is a self-contained Unix computer with a powerful Intel i860 CPU. All computations take place on this card, as the host PC CPU is only used to communicate with this card. This hardware greatly accelerates computation. For instance, a Fourier transform (used extensively in image correlation) is calculated ~40 times faster than on the PC currently used for correlation.

b. JEOL 6400 SEM with PC-Motorized Controls

This SEM is fully computerized. The SEM computer accepts external control via a RS232 interface, and currently accepts 120 ASCII format commands. It has a 1024 by 1024 pixel digital-image framestore, and the vendor supplies a PC-interface card to receive the image from the SEM framestore. A PC and motorized controls compose a SEM stage automation package. Stage control is by the PC keyboard, joystick, or by remotely issued ASCII format commands issued from the central computer via a RS232 interface.

C. Development of Improved Authentication Algorithms

One of the most time-consuming authentication computations is the overlay of the baseline and field-inspection casting images. The present algorithm is based on correlations performed in Fourier space, as described in Appendix A. Neural network-based algorithms can be much more efficient. A neural network image

overlay algorithm would be written in either Fortran or C languages and be integrated into the Semper language as a user-written command.

Currently, authentication is determined by use of the linear correlation and local-sum statistics. Alternate statistical methods should be systematically analyzed to determine if they are superior. Examples of alternate statistics are a spatial-frequency weighted correlation or the Hamming distance.

D. Improved Adversary Analysis

An improved adversary-analysis must rationally evaluate the plastic-casting intrinsic-surface tag. The three areas that need additional effort are discussed in detail in Section VI.B.1. Specifically a realistic authentication exercise, validated image-alignment software, and a full replication should be performed.

An improved authentication exercise would be based on a realistic generic treaty implementation of the tag. This exercise would realistically segregate the tasks of the inspecting and inspected sides of a treaty. As the tag demonstrator, ANL would be the inspecting side, and the adversary analyst would be the inspected side. The adversary would present unmarked original surfaces to ANL. ANL, as the inspecting side, would mark the surfaces and make the baseline castings. Then, ANL would return the original surfaces to the adversary. The adversary would then fabricate the positive-replica surfaces. ANL, as the inspecting side, would then make castings from pairs of surfaces presented to it by the adversary. These surfaces could be either the original or replicate surfaces. Castings made from these surface pairs would be the field-inspection castings. ANL would then authenticate the surfaces by comparing the field-inspection and baseline castings.

A rigorous test of both ANL and the adversary analyst alignment software must be performed before additional analyses are begun. One way to proceed is to have ANL and the adversary analyst submit pairs of digital data sets to each other. There must be translation, rotation, and magnification differences between most of the pairs of data sets. One image in each pair should be designed as the baseline. Specific 128 by 128 pixel baseline subregions should be identified for comparison by supplying a list of the central x,y coordinates of each subregion. The software would be considered validated when correlation values agree to the third decimal place.

It should be appreciated that high-quality positive replicas are needed to determine the amount of data needed to authenticate each surface. This amount must be known to specify a high-throughput authentication system as discussed in Section VII.B.1.

Full replication requires that an inspector cannot visually distinguish the positive-replica material from the original TLI surface. Specifically, the positive replica must appear to have the same reflectance and color as the original TLI surface. If the chosen original surface is metallic, the adversary analyst must prepare metallic positive-replicas to complete the replication. Moreover, the adversary must also demonstrate that a metallic positive-replica can be seamlessly blended into a larger metal surface.

E. Application-Specific Environmental Testing

Specific applications may involve environmental challenges to the stability of the controlled-item surface. This should be evaluated on a case-by-case basis, and appropriate testing performed to qualify the use of the surface. In addition, various protective coverings such as the bar-code label would be tested. It is also important to have qualified corrosion/weathering experts perform the environmental testing. This testing must be accelerated to qualify this tag for long-term service.

VIII. DISCUSSION

A. Implementation of Unique Surface Tag Authenticated by an SEM

1. Implementation Options

ANL investigated three options to implement a unique surface tag authenticated by an SEM. These options differ in whether the surface topography is directly or indirectly captured and where the SEM is located.

2. On-Site Direct SEM Authentication

The first option is to directly attach the SEM electron-optics column to the tagged item. This has the advantage that the tag-surface elemental composition, distribution of composition, as well as surface topography can be used for authentication. Another advantage is that authentication could be made while the SEM is still attached to the item. One disadvantage is the fieldable-SEM spatial resolution is not as good as a commercial laboratory SEM.

ANL constructed a proof-of-concept SEM with an electron-optics column attached to a simulated item [14]. Design issues addressed by the proof-of-concept SEM included column-item vacuum sealing, differential column pumping, and vibration sensitivity. A 1-micron spatial resolution was demonstrated.

ANL also designed a fieldable SEM [15]. The electron-column design included both unique power-saving permanent as well as standard electromagnetic lenses. Prototype condenser and objective lenses were built and tested to prove the design. Other major system components were selected. Estimated total-system weight was 52-Kg including a 7-Kg electron column. A 0.1-micron spatial resolution was estimated for this SEM.

3. On-Site Indirect Authentication

The second option is to indirectly capture the surface topography with a casting and subsequently authenticate the casting with an on-site SEM. This SEM could be transported to the inspection site in a van. The main advantage is the casting could be authenticated in the field. One disadvantage is that the authentication could not be based upon composition. There is a commercial, transportable, 0.5-micron resolution SEM that could be adapted for this application [15]. If there is renewed interest in on-site indirect authentication, the SEM design should be evaluated. It is likely that a much-better spatial resolution could be attained.

4. Central-Laboratory Indirect Authentication

The third option is to indirectly capture the surface topography with a casting and then authenticate the casting in a central laboratory a few days later. One advantage is the highest-resolution, commercial SEM could be used for the casting examination. The resolution of a commercial field-emission gun SEM could be as small as 0.001-microns. Other advantages and the disadvantages are discussed below. Of course, this third option is the plastic-casting intrinsic-surface tag that is the focus of this report.

B. Categorization and Usage of Tags

Specific tagging concepts can be placed into at least three categories. Moreover, tags can be used in either overt or covert modes.

The first category is whether the tag is intrinsic or attached. Intrinsic tags utilize a unique feature of the controlled item. Attached tags use some externally-created unique feature which must be bonded to the item.

The second category is whether the tag is active or passive. Active tags require power sources such as batteries. Passive tags require no electrical power. However, it should be emphasized that the reader for a passive tag may require electrical power.

The third category describes whether each tag is unique to each item in a particular controlled group, or whether each tag is just unique to the group. A tag unique to each item is called an individual-item tag, and a tag unique only to a group of items is called a class tag.

A tag can be used in either an overt or covert mode. An arms-control treaty tag is an example of the overt mode. In the overt mode the inspected side may not accept a tag unless its technology is fully understood. For the overt mode both the tag and its reader can be conspicuous. There are also potential uses for covert-mode tags. In the covert mode the tag technology is known only by the inspecting side, and the tag must be inconspicuous. For some covert-mode uses the reader must also be inconspicuous.

C. Comparison of Tag Concepts

Reference 16 summarizes a group of tag and seal concepts developed by DOE for arms-control treaty applications. Table 3 describes four tag concepts selected from this group. These concepts are the plastic-casting tag, ultrasonic-intrinsic tag, reflective-particle tag, and the electronic-identification device.

These four concepts necessarily use more advanced technology than less-secure commercial tags. The advanced technology is required because it must be assumed that the inspected side would have long periods of sole access to the tag. It was also assumed that the inspected side would have resources equivalent to national laboratories to attempt tag duplication.

The plastic-casting, ultrasonic-intrinsic, and reflective-particle tags are image based in the sense that they rely upon unique two-dimensional patterns obtained from random microscopic features. Both a casting and a scanning-electron beam are used to image the microscopic surface-topography for the plastic-casting tag. For the ultrasonic-intrinsic tag a scanning, acoustic, pulse-echo reader is used to image sub-surface variations in material density or elastic modulus. The reflective-particle tag utilizes visible light illumination reflected by small multi-faceted particles. A separate image is read by a camera for each illumination angle. There may be as many as 21 illumination angles.

During each inspection for the plastic casting, ultrasonic intrinsic, and reflective-particle tags, data sets (images) containing three-dimensional information are obtained. Tag authenticity is determined by comparing baseline and field-inspection data sets. These data sets are compared by some form of correlation, although other numerical comparisons may be made.

Table 3

Comparison of Four Tag Concepts

Name	Unique Feature	Electronic Reader Attached to or Near Controlled Item	Authenti-cation Location	Intrinsic (I) or Attached (A)	Passive (P) or Active (A)	Individual - Item (I) or Class (C)	Developing Laboratory
Plastic Casting Tag	Surface Topography	No	Central Laboratory	I	P	I	Argonne
Ultrasonic Intrinsic Tag	Sub-surface Density and Elastic Inhomogeneities	Yes	On-site	I	P	I	Pacific Northwest
Reflective Particle Tag	Reflectance of Small Multifaceted Particles Sequentially Illuminated from Multiple Directions	Yes	On-site	A	P	I	Sandia
Electronic Identification Device	Cryptographic Key	Yes	On-site	A	A	I or C	Lawrence Livermore

The electronic identification device uses a cryptographic key as the unique identifier. This key is a binary number over 100 bits long. Both the microchip circuitry in this device and its reader have the key. During the inspection the reader sends a random number to the device. The cryptographic key in the device encrypts this number. Then the device sends a numerical response back to the reader. This response is unique to the key. Since the reader also has the key it can then verify that the device is giving the correct response.

Electronic reader technology is used for the ultrasonic-intrinsic tag, reflective-particle tag, and electronic-identification device. These electronic readers must be attached or in close proximity to the controlled item when the tag is read.

The plastic-casting tag is read by a two step process. In the first step a non-electronic reader is used. This fielded reader is a human with a container of solvent and a strip of casting tape. The fielded reader makes a casting of the tag surface. For the second step the casting is brought back to a central laboratory where it is authenticated with the SEM images.

Authenticity is determined during the on-site inspection for the ultrasonic-intrinsic tag, reflective-particle tag, and the electronic-identification device. On-site determination of authenticity requires bringing the baseline data or key to the inspection site. In addition fieldable authenticators attached to or built into the readers must be brought to the inspection site.

For the plastic-casting tag authenticity is determined a few days after the inspection. The castings gathered in the inspection are brought to a central laboratory where the baseline data, SEM casting-reader, and authenticating computer are located.

The plastic casting and ultrasonic tags are intrinsic. Both the reflective-particle tag and the electronic-identification device are attached.

The plastic casting, ultrasonic intrinsic, and reflective-particle tags are passive. Only the electronic-identification device is active. There are several activity options for this device. This device can be active all the time or only active when being read.

Plastic casting, ultrasonic intrinsic, and reflective-particle tags are always individual-item tags. The electronic identification device can be an individual-item tag if a unique cryptographic key is associated with each device. However, if the same key is used for a set of devices used on a particular group of items then the electronic-identification device is a class tag.

D. Plastic-Casting Tag Advantages

1. Transfer Resistance

One way to defeat a tag is to transfer a legitimate tag to an illegal or uncontrolled item. Because the plastic-casting tag is intrinsic, it does not have a bonded interface with the controlled item. The lack of an interface makes intrinsic tags less vulnerable to transfer than attached tags.

2. No Electronics in Fieldable Reader

For some controlled items proximity to or contact with an electronic reader may raise safety or intelligence concerns. Field reading the plastic-casting tag only requires a human, container of solvent, and casting tape in proximity to or contact with the controlled item. Of course, the protective label and casting bar-codes would not be read by the electro-optic Laser-Wand bar-code reader-computer for these applications. Rather, the inspector would enter the enter alpha-numeric information on inspection forms by hand.

3. Inconspicuous Tag for Covert Mode

Because the plastic-casting tag is intrinsic, it can be inconspicuous. Obviously, the protective bar-code label would not be used. A secure internal-surface can provide tag protection, or protection can be designed into the controlled item. Moreover, a decision to roughen the surface would have to be made on a case-by-case basis, as roughening may reveal the item is tagged. Most as-manufactured surfaces have authenticatable topography, but this topography may be easier to duplicate. However, the tag owner has the advantage of knowing the exact tag location. Therefore, even if an adversary learns an item is tagged, duplication of all potential tag sites on even one controlled item is a formidable task.

4. Simple Fieldable Reader for Covert Mode

For covert tagging in most instances, the lack of electronics and simplicity of the fieldable plastic-casting tag reader are advantages. The inconspicuous fieldable reader consists of a human, casting tape, and a container of solvent.

5. Central-Laboratory Authentication Advantages

The plastic-casting tag is authenticated at a central laboratory. Compared to on-site authentication this can allow a longer time for data collection and calculating authenticity. The baseline data is also kept in the central laboratory. Authentication with a much larger amount of data per tag is practical compared to tags that must bring baseline data to the inspection site.

For overt mode applications there may also be protocol advantages to authenticating off-site. The on-site inspectors need only perform routine functions. These inspectors would never have to deal with complications that might arise after informing the inspected side of a non-genuine tag.

Central-laboratory authentication may be preferred for its economic advantages. All the expensive equipment is kept in a single location where it can be conveniently operated and maintained.

6. Well-Known Replication Technology

Replication [17] is a technology widely used by microscopists. Cellulose-acetate plastic castings represent just one of a variety of replication techniques. Consequently, replication is well known and understood. Knowledge of replication could promote acceptance of this tag by an adversary. Understanding of replication should give confidence that this tag is viable.

7. Well-Known SEM Technology

The SEM [10] is a very sophisticated device used for a variety of purposes in research and manufacturing. Compared to other tag readers (except the microchip based electronic-identification device) more effort and money have been spent on developing the basic technology. There is also a vast body of knowledge on SEM imaging and an appreciation of its advantages. Knowledge and understanding of the SEM can also promote acceptance of this tag by an adversary.

8. First-Principle Approach to Tag Duplication

The plastic-casting tag uses a first-principle approach to assessing tag duplication. This principle is the modulation transfer function. Both imaging and signal processing theory use this function as an accepted first-principle. This approach lends confidence to tag viability.

9. Restriction on Candidate Duplication Technologies

Candidate tag duplication technologies must have resolutions near to or smaller than the authentication-image pixel size. The plastic-casting tag authentication-image pixel size is about 0.03-microns. This dimension is orders of magnitude smaller than the pixel size of other image-based tags. The small pixel size of the plastic-casting tag restricts the choice of duplication technologies.

E. Plastic-Casting Tag Disadvantages

1. No On-Site Authentication

The plastic-casting tag does not provide on-site authentication. For an illegal item non-authenticity would be determined in a central laboratory a few days after the inspection. If protocol allowed an immediate follow-up inspection, the adversary would have time to move the legitimate controlled-item to the inspection site.

2. Sensitivity to Corrosion and Weathering

The plastic-casting tag is sensitive to corrosion or weathering of the controlled item surface. For long-term overt-mode use in an environmentally-challenging environment this tag depends on the preservation provided by its protective cover. Long-term covert-mode usage in an environmentally challenging environment may require that protection be designed into the controlled item.

3. Protective Cover Required during Normal Operations

For the overt mode the protective cover could be an impediment to normal operation of the item.

IX. ACKNOWLEDGMENTS

The ANL tag project gratefully acknowledges the support extended by the U.S. Department of Energy, Office of Nonproliferation and National Security. DOE Program Managers during the span of the project were Howard Heu, Dr. James Fuller, and Chris Makris.

At Argonne, Arms Control Program Manager Dr. Armando Travelli and Dr. Linda Gaines provided valuable guidance. The replication and microscopical expertise of Dr. Nestor Zaluzec was extremely valuable. Mr. R. C. Haglund and Dr. A. Purohit participated in exploratory work on different casting materials. Mr. C. A. Morse contributed to the replication experiments. Dr. J. A. Morman contributed to the initial work on numerical authentication. Dr. J. W. Holland provided initial technical program planning. Drs. P. S. Maiya and T. F. Kassner provided guidance on corrosion. Dr. R. H. Howes of Ball State University performed a field test.

X. REFERENCES

1. R. G. Palm and A. DeVolpi, *Intrinsic-Surface-Tag Image Authentication*, Argonne National Laboratory Report ANL/ACTV-91/5 (December 1991).

2. A. DeVolpi, *Understanding Correlation Coefficients in Treaty Verification*, Argonne National Laboratory Report ANL/ACTV-91/4 REVISED (February 1993).

3. P. S. Maiya and T. F. Kassner, *Role of Atmospheric Corrosion of Aluminum Alloys in Viability of Intrinsic-surface Methods for Tagging Military Hardware*, Argonne National Laboratory Report ANL/ACTV-91/6 (November 1991).

4. W. J. Smith, *Modern Optical Engineering*, McGraw-Hill, New York (1966), pp. 308-325.

5. R. L. Courtney, Sandia National Laboratory, private communication, June 1993.

6. W. W. Saylor and J. L. Rink, *Final 1991 SEM Red Team Report* (unclassified title), Los Alamos National Laboratory Arms Reduction Treaty Verification Programs, N-DO/SG-91:150C (Sept. 1991).

7. A. DeVolpi and R. G. Palm, *Technical Response to the Final 1991 SEM Red-Team Report* (unclassified title), Argonne National Laboratory Arms Control Program 275-92, Feb. 1992.

8. C. R. Mansfield, *Vulnerability Assessment of the Scanning Electron Microscope Plastic Casting Tag* (unclassified title), Los Alamos National Laboratory Report LA-CP-93-121 (April 1993).

9. C. R. Mansfield, *Vulnerability Assessment of the Scanning Electron Microscope Plastic Casting Tag*, Los Alamos National Laboratory Report LA-UR-93-1900 (May 1993).

10. J. I. Goldstein, D. E. Newbury, P. Echlin, D. C. Joy, C. Fiori, E. Lifshin, *Scanning Electron Microscopy and X-ray Microanalysis*, Plenum Press, 1981.

11. *SPSE Handbook of Photographic Science and Engineering*, John Wiley and Sons, 1973, p. 947.

12. J. L. Rink, Los Alamos National Laboratory, personal communication, June 1991.

13. E. Ko, Argonne National Laboratory, personal communication, February 1995.

14. R. G. Palm, N. J. Zaluzec, A. Purohit, J. A. Morman, A. DeVolpi, and J. E. Mitrani, *Unique Tamper-revealing Tags for Arms Control Verification: Electron Microanalytical Authentication of TLI Intrinsic Surface Labels*, Argonne National Laboratory Report ANL/ACTV-89/1 (January 1989).

15. N. J. Zaluzec, A. Philippedes, R. G. Palm, A. DeVolpi, and J. W. Holland, *Intrinsic TLI Surface Tag Directly Authenticated by a SEM (Closeout Report)*, Argonne National Laboratory Report ANL/ACTV-91/3 (November 1991).

16. *Verification Technologies*, DOE Report DOE/DP/OAC/VT-92B, 3rd Quarter 1992.

17. J. H. M. Willison and A. J. Rowe, *Replica, Shadowing and Freeze-Etching Techniques*, North-Holland Publishing Co., Amsterdam, Netherlands, 1980.

APPENDIX A. CONTROL-SYSTEM AND SIGNATURE-CORRELATION SOFTWARE

1. Introduction

Programs for linear-correlation coefficient and local-sum mean signature determination are described in this appendix. The gray-scale and binary-image processing has been implemented in the Semper 6.2 image-processing software. This software is a trademark of Synoptic's Ltd. Semper is a general-purpose image-processing program. Commands used for such diverse image-processing tasks as correlation, particle-size analysis, and remote sensing of satellite images illustrate Semper's capabilities. The commands can be entered individually in the interactive mode, or interpreted programs can be written using the commands and the logical testing capabilities provided in the Semper language.

2. Image Registration and Correlation

Image matching must register two as-acquired casting images using image correlation software. For two digitized images, registration is achieved when the x,y addresses of each image correspond to the same points on the surface being compared. In general, two digitized images of the same or similar surfaces are dissimilar if both surfaces can not be identically positioned with respect to the imaging device. These dissimilarities can be described either as translation, rotation, or magnification differences. In the case of the digitized images used for this authentication method all these dissimilarities must be corrected before the images can be scored. The registration software calculates many linear correlation coefficient (LCC) values as it searches for the minimum difference. At the minimum difference the LCC is maximized. This maximum LCC is also used as part of the score. Most of the computational effort (~90%) to score the images is spent in registration.

A program has been written that uses three important Semper commands to accomplish registration by image correlation. The software uses standard Fourier techniques to accomplish registration. Fourier techniques are used because they are more computationally efficient for the large-size images being compared. The Fourier-transform based correlation command (XCF) effectively translates two images over each other and reports the Δx and Δy translations that provide the best registration. The best registration is determined from the peak linear correlation coefficient amongst all the translations. In general, N^2 registration correlations are calculated for input images of size N by N. Another Semper correlation command (OCF) determines the rotational correlation between two images. OCF, as implemented in this program, operates on the real images but can also be implemented on their Fourier power spectra. The last important command (EXTRACT) computes a translated, magnified, and rotated subimage from an as-acquired image using bilinear interpolation.

The program implements registration in the following manner. One input subimage (e.g., 128 x 128 pixel size) is simply extracted from the first source image, which is typically 512 x 512 pixels. A second subimage is constantly being extracted from the second source image. The program attempts to find the optimum extraction of the second subimage. This extraction is determined by a search for peak registration of the two subimages, and it is accomplished in three steps. The first step determines a translation-registered second subimage. This image is used to start the magnification search for the second step. A translation and magnification registered second subimage is determined upon concluding this step. This subimage is used as input to the third step. The third step corrects for rotational differences. The output of the third step is the maximum LCC between the first and second subimages since it has been corrected for all differences. This correlation is computed to within a 0.5 pixel shift and a 0.1 degree rotation of the theoretically best registration. It provides a maximum LCC accurate to at least the third decimal point of the theoretically best registration. It is important to note that casting images from original surfaces could be registered by a less computationally-intensive process. However, registration of the original and replica images is complicated by the presence of false maximum correlations, so more calculations are required to assure that the true maximum is found. Another important detail is that the magnification and rotation steps sometimes require an additional translation correction to maximize the LCC. If this is required, the additional translation correction is implemented within the magnification and rotation steps.

Table 4 is the Semper source listing for the correlation program MATCHIM, and Table 5 shows a sample output for this program.

Table 4

Semper Source for Image Correlation Program MATCHIM

```
Matchim()
TIME RESET
PAGE NOPROMPT
!PROGRAM MATCHIM IS WRITTEN TO OVERLAY TWO IMAGES
!WITH STRONG DIRECTIONAL COMPONENTS SUCH AS IMAGES
!OF SCRATCHES RUNNING IN ONE DIRECTION.
!NOTE THE IMAGES ALSO NEED A STRONG DIRECTIONAL COMPONENT.

LOCAL SZ1,II1,XX1,XX2,IO1,II2,XX2,YY2,IO2,TP,TM,TRP,TRM
LOCAL T1,T2,T3,T4,T5,A,B,KE,KRE,SZ2,SF1,ORD,IRD,TH1,TH2,DEL
LOCAL X2,Y2

ASK 'SIZE OF OVERLAID OUTPUT IMAGES? ' SZ1

!FIRST OUTPUT IMAGE EXTRACTED FROM FIRST INPUT
!IMAGE AT INPUT COORDINATES.

ASK 'FIRST INPUT IMAGE FOR OVERLAY ' II1
ASK 'X,Y POSITION IN FIRST INPUT IMAGE ' XX1,YY1
ASK 'OUTPUT IMAGE NUMBER AS EXTRACTED FROM FIRST IMAGE ' IO1

!SECOND OUTPUT IMAGE IS EXTRACTED FROM SECOND
!INPUT IMAGE AFTER OPTIMUM SHIFT, MAGNIFICATION
!AND ROTATION CORRELATION IS DETERMINED.

ASK 'SECOND INPUT IMAGE FOR OVERLAY ' II2
ASK 'X,Y POSITION IN SECOND INPUT IMAGE ' XX2,YY2
ASK 'OUTPUT IMAGE NUMBER FROM SECOND IMAGE ' IO2
X2=XX2
Y2=YY2
DEL 4001,4999

COPY II2 4001

CREATE 4002 SIZE SZ1 BYTE
EXTRACT II1 4003 SIZE SZ1 POS XX1,YY1
ORIGEN 4003 RESET
COPY 4003 IO1
FOU 4003

TYP 'DOING INITIAL SHIFT SEARCH FOR A COMMON CENTRAL PIXEL'
FOR K=1,5
  EXTRACT 4001 4002 SIZE SZ1 POSITION XX2,YY2
  ORIGEN 4002 RESET
  XCF 4003 WITH 4002 TO 4990
  IF X=0 & Y=0 JUMP MG1
  XX2=XX2+X
  YY2=YY2+Y
LOOP
TYP 'CAN'T GET X=Y=0 SHIFT CORRELATION IN 5 TRIES, X,Y= ',X,Y
```

Table 4 (continued)

Semper Source for Image Correlation Program MATCHIM

```
MG1:
! T1 IS TMAX FOR INITIAL SHIFTING
T1=T

TYP 'DOING MAGNIFICATION ADJUSTMENT'
A=1
EXTRACT 4001 4002 SIZE SZ1 POSITION XX2,YY2 SAMPLING (1+(.5/SZ1))
ORIGEN 4002 RESET
XCF 4003 WITH 4002 TO 4990
TP=T

EXTRACT 4001 4002 SIZE SZ1 POSITION XX2,YY2 SAMPLING (1-(.5/SZ1))
ORIGEN 4002 RESET
XCF 4003 WITH 4002 TO 4990
TM=T

IF TP<TM A=-1

T2=T1
SZ2=ROUND(SZ1/8)
FOR K=1,SZ2
 KE=K
 EXTRACT 4001 4002 SIZE SZ1 POSITION XX2,YY2 SAMPLING +
 (1+((A*K)/SZ1))
 XCF 4003 WITH 4002 TO 4990
 XX2=XX2+X
 YY2=YY2+Y
 IF T<T2 JUMP MG2
 ! NOTE WHEN K=KE-1, T=TMAX, SO T2=TMAX AT JUMP TIME
 T2=T
LOOP
TYP 'UNABLE TO FIND MAGNIFICATION ADJUSTMENT, WITHIN 12% LIMIT'
RETURN

MG2:

! TYP 'DOING FINE MAGNIFICATION ADJUSTMENT'
SF1=1+((A*(KE-1))/SZ1)
! SF1 ABOVE IS THE SAMPLING FACTOR THAT GAVE
! THE PEAK CORRELATION IN LABEL MAG1
! WHICH PROVIDED CRUDE MAGNIFICATION ADJUSTMENT
SF1=SF1+.5/SZ1
EXTRACT 4001 4002 SIZE SZ1 POSITION XX2,YY2 SAMPLING SF1
ORIGEN 4002 RESET
XCF 4003 WITH 4002 TO 4990
T3=T
IF T3>T2 JUMP ROT

SF1=SF1-1.0/SZ1
EXTRACT 4001 4002 SIZE SZ1 POSITION XX2,YY2 SAMPLING SF1
ORIGEN 4002 RESET
XCF 4003 WITH 4002 TO 4990
T3=T
IF T3>T2 JUMP ROT
```

Table 4 (continued)

Semper Source for Image Correlation Program MATCHIM

```
SF1=SF1+.5/SZ1
EXTRACT 4001 4002 SIZE SZ1 POSITION XX2,YY2 SAMPLING SF1
ORIGEN 4002 RESET
T3=T2

ROT:


TYP 'DOING ROTATIONAL CORRELATION, INITIAL OCF ANGLE FOLLOWS:'
! T3 AND SF1 ARE SET COMING INTO ROTATE AS THE PEAK
! CORRELATION AFTER MAGNIFICATION ADJUSTMENT,
! AND THE SAMPLING FACTOR THAT PROVIDES THE
! PEAK CORRELATION.
ORD=(SZ1/2)-1
IRD=1
OCF IO1 WITH 4002 TO 4999 FULL RINGS 25 RAD IRD,ORD VER
TYP 'OCF THETA= ',DEG(THETA),' DEGREES ',THETA,' RADIANS'

TH1=THE
DEL=(.1/180)*PI
B=1

EXT 4001 4002 SIZ SZ1 POS XX2,YY2 SAM SF1 ANG TH1
ORIGEN 4002 RESET
XCF 4003 WITH 4002 TO 4990
T4=T
EXT 4001 4002 SIZ SZ1 POS XX2,YY2 SAM SF1 ANG TH1+DEL
ORIGEN 4002 RESET
XCF 4003 WITH 4002 TO 4990
TRP=T

EXT 4001 4002 SIZ SZ1 POS XX2,YY2 SAM SF1 ANG TH1-DEL
ORIGEN 4002 RESET
XCF 4003 WITH 4002 TO 4990
TRM=T
IF TRP<TRM B=-1

T5=T4
FOR K=1,15
 KRE=K
 EXT 4001 4002 SIZ SZ1 POS XX2,YY2 SAM SF1 ANG (TH1+B*K*DEL)
 ORIGEN 4002 RESET
 XCF 4003 WITH 4002 TO 4990
 IF T<T5 JUMP DONE
 T5=T
 XX2=XX2+X
 YY2=YY2+Y
LOOP

TYP 'COULDN'T FIND ANGLE TO ROTATE OPTIMALLY IN 15 TRIES'
TYP 'XX2,YY2= ',XX2,YY2,'T5= ',T5
TYP 'XX2,YY2= ',XX2,YY2,'T5= ',T5
```

Table 4 (continued)

Semper Source for Image Correlation Program MATCHIM

```
DONE:


TH2=TH1+B*(KRE-1)*DEL
EXT 4001 4002 SIZ SZ1 POS XX2,YY2 SAM SF1 ANG TH2
ORIGEN 4002 RESET
COPY 4002 IO2

TYP ''
TYP 'FINAL CORRELATION AFTER MAGNIFICATION+ROTATION= ',T5
TYP 'INITIAL SHIFT, FINAL MAGNIFICATION CORRELATIONS ',T1,',',T3
TYP 'OUTPUT IMAGE SIZE, FINAL SAMPLING(1/MAG.) FACTOR= ',SZ1,',',SF1
TYP 'FINAL X,Y EXTRACTION COORDINATES FOR SECOND IMAGE= ',+
XX2,',',YY2
TYP 'FINAL ROTATION ANGLE ',DEG(TH2),' DEGREES ',TH2,'RADIANS'
TYP ''
TYP 'EXAMINE FIRST INPUT IMAGE'
EXAMINE II1
TYP +
'INITIAL+FINAL X,Y COORDINATES FOR FIRST INPUT IMAGE ',XX1,',',YY1
TYP 'FIRST OUTPUT IMAGE NUMBER, ',IO1
TYP ''
TYP 'EXAMINE SECOND INPUT IMAGE'
EXAMINE II2
TYP 'INITIAL X,Y COORDINATES FOR SECOND INPUT IMAGE ',X2,',',Y2
TYP 'SECOND OUTPUT IMAGE NUMBER ',IO2
TYP ''
TYP +
'ESC INDICES FROM MG1,ROT; A,B SEARCH DIR VAL ',KE,'+
,',KRE,';',A,',',B
TIME NOVER
TYPE 'PROGRAM TIME= ',FIX(T/60),' MIN ',REM(T,60),'SEC'
PAGE PROMPT
end
```

Table 5

Sample Output of Semper Program MATCHIM

```
FINAL CORRELATION AFTER MAGNIFICATION+ROTATION= 0.904789
INITIAL SHIFT, FINAL MAGNIFICATION CORRELATIONS 0.875711,0.903493
OUTPUT IMAGE SIZE, FINAL SAMPLING(1/MAG.) FACTOR= 128,0.980469
FINAL X,Y EXTRACTION COORDINATES FOR SECOND IMAGE= -7,95
FINAL ROTATION ANGLE -0.466315DEGREES -0.00813874RADIANS

EXAMINE FIRST INPUT IMAGE
 5041 Size 641,480,1 300.5kb Image Byte wp
    j814000
INITIAL+FINAL X,Y COORDINATES FOR FIRST INPUT IMAGE -96,47
FIRST OUTPUT IMAGE NUMBER, 5941

EXAMINE SECOND INPUT IMAGE
 5042 Size 641,480,1 300.5kb Image Byte wp
    j824000
INITIAL X,Y COORDINATES FOR SECOND INPUT IMAGE -8,95
SECOND OUTPUT IMAGE NUMBER 5942

ESC INDICES FROM MG1,ROT; A,B SEARCH DIR VAL 4,3;-1,-1
PROGRAM TIME= 9 MIN 45.45 SEC
```

3. Local-Sum Program

The local-sum mean program LOCSUM prompts for two registered gray-scale images as input, and for the percent of the brightest pixels desired in the thresholded images. The program then searches the histograms of the input images to provide binary images thresholded closest to the desired brightness percent. There is a minor implementation problem since, in general, the binary images will not have exactly the same brightness percentage, nor will either brightness percentage be equal to that requested in the input. Typically, if 15% brightness is used as the desired input threshold value, then the binary images might have 14-16% of their pixels set to one. These different percentages of bright pixels causes minor increases in the means of the absolute difference and local-sum images. However, this implementation problem does not affect the ability of the means to discriminate original from replica tag images.

After the binary images are obtained, the steps necessary to calculate the mean of the absolute-difference image and the local-sum image are straightforward.

Table 6 is the Semper code source listing for program LOCSUM, and Table 7 presents a sample output for this program.

Table 6

Semper Source for Binary Image Processing Program LOCSUM

```
Locsum()
TYP 'THIS PROGRAM  CALCULATES  THE LOCAL-SUM  MEAN FROM TWO GRAY'
TYP 'IMAGES THRESHOLDED  TO THE BRIGHTEST  FRAC OF PIXELS'
del 4001,4999
ASK 'INPUT IMAGES TO THRESH. ,BRIGHTEST  FRAC. TO THRESH. 'II1,II2,BT
! need histogram to develop threshold
HISTOGRAM  II1 TO 4101 FP
! max,mn1 is min pixel value in input image
MN1=MIN
! max is maximum gray level in input image
! d1 is size of histogram file
D1=MAX-MIN+1
!pcb sets nco and nro of input image
PCB II1
!extract out only the histogram part of the histogram file
!last two values in histogram file are min,max, respectively,
EXT 4101 SIZ D1,1 LEF
!next steps integrate the histogram starting at the lowest gray value
SUM=0
FOR I=0,D1-1
  SUM=SUM+P(I)
  P I=SUM
LOOP
!next step normalizes the integration so values are from 0 to 1
CAL 4:101/(NRO*NCO)
!next step produces a file peaked at desired brightness fraction
CAL 1-MOD(4:101-(1-BT)) TO 4102
! peak command records the peak position in plist 4103
PEAK 4102 4103
!xh1 is x address of peak
XH1=P(0,0,0)
!mn1+xh1 give the desired gray level to attain a binary
!thresholded to the brightest bt1 fraction
CAL :II1>(MN1+XH1) TO 4104
SEL 4101
AB1=P(XH1)
DEL 4101,4103
COPY 4104 BYTE
COM DEV 4 NOVER
```

Table 6 (continued)

Semper Source for Binary Image Processing Program LOCSUM

```
!GET THRESHOLDED  IMAGE FOR II2
HISTOGRAM  II2 TO 4105 FP
MN2=MIN
D2=MAX-MIN+1
EXT 4105 SIZ D2,1 LEF
SUM=0
FOR I=0,D2-1
  SUM=SUM+P(I)
  P I=SUM
LOOP
CAL 4:105/(NRO*NCO)
CAL 1-MOD(4:105-(1-BT))  TO 4106
PEAK 4106 4107
XH2=P(0,0,0)
CAL :II2>(MN2+XH2) TO 4108
SEL 4105
AB2=P(XH2)
DEL 4105,4107
COPY 4108 BYTE
COM DEV 4 NOVER

!AT THIS POINT 4104 AND 4108 CONTAIN THE BINARY IMAGES
!THAT THE LOCAL-SUM MEAN WILL BE CALCULATED  FROM
!CALCULATE  ABSOLUTE  DIFFERENCE  BINARY FROM BRIGHTNESS  THRESHOLDED
!BINARIES
CAL MOD(4:104-4:108) TO 4009
SURVEY  4009 FULL NOVER
MAD=MEA

!CREATE  KERNAL  LOCAL PIXEL  WEIGHTING  IMAGE  TO USE WITH FIR COMMAND
CREATE  4010 SIZE 3,3 VALUE  1

!FORM  LARGE  LOCAL-SUM  IMAGE
FIR 4009 TO 4011 WITH 4010
!EXTRACT  A LOCAL-SUM  WITHOUT  BORDER  PIXELS OF LARGE  LOCAL-SUM  IMAGE
EXT 4011 SIZ NCO-2,NRO-2
SURVEY  4011 FULL NOVER
MLS=MEA

TYP ''
TYP 'LOCAL-SUM MEAN= ',MLS
TYP ''
TYP 'MEAN ABS DIFF IMAGE= ',MAD
TYP 'ACTUAL BRT THR IMAGES  1 AND 2 ARE  = ',1-AB1,1-AB2
end
```

Table 7

Sample Output of Semper Program LOCSUM

```
LOCAL-SUM MEAN= 0.586357

MEAN ABS DIFF IMAGE= 0.0649414

ACTUAL BRT THR IMAGES 1 AND 2 ARE = 0.1512450.143188
```

APPENDIX B. COMMERCIAL COMPONENTS PARTS LIST

1. Scanning Electron Microscope

   Model: JSM 5300

   Vendor: JEOL USA
   11 Dearborn Road
   Peabody, Massachusetts 01960

   Phone: 508-535-5900

2. Sputter Coater

   Model: Hummer VII

   Vendor: Anatech Ltd.
   5510 Vine Street
   Alexandria, Virginia 22310

   Phone: 703-971-9200

3. Image Processing Hardware

   Model: Quantimet 520

   Vendor: Leica Inc.
   11 Deer Lake Road
   Deerfield, Illinois 60015

   Phone: 708-405-0123

4. Image Processing Software

   Software: Semper 6.3

   Vendor: Synoptics Ltd.
   164 CJC Highway
   Cohasset, Massachusetts 02025

   Phone: 617-383-2289

5. Portable Bar Code Reader/Computer

   Model: Laser-Wand

   Vendor: Hand Held Products
   8008 Corporate Center Drive
   Charlotte, North Carolina 28226

   Phone: 704-541-1380

Distribution

Internal:

R. G. Palm (16)
A. DeVolpi (5)
L. W. Deitrich
D. P. Weber
C. E. Dickerman
L. L. Gaines
G. S. Stanford
A. Travelli
R. R. Rudolph
T. F. Kassner
P. S. Maiya
N. J. Zaluzec
J. W. Holland
RE Experimental Physics Section File: C
RE File: 54920-20
TIS Files

External:

DOE/OSTI (2)
ANL-E Library (2)
ANL-W Library
Manager, Chicago Operations Office, DOE
M. F. O'Connell, Office of Nonproliferation and National Security, U.S. Department of Energy, Washington, DC
C. M. Makris, Office of Nonproliferation and National Security, U.S. Department of Energy, Washington, DC
S. J. Rudnick, Office of Nonproliferation and National Security, U.S. Department of Energy, Washington, DC
J. Fuller, PNL
N. Hansen, PNL
R. L. Courtney, SNL
K. M. Tolk, SNL
R. Scarlett, LANL
R. G. Johnston, LANL
M. Riley, LLNL
R. H. Howes, Ball State University